AD-A080 177 AIR FORCE INST OF TECH WRIGHT-PATTERSON AFB OH SCHOO--ETC F/6 7/4
EFFECTS OF SULFURHEXAFLUORIDE ON IONIZATION WAVES IN AN ARGON G--ETC(U)
DEC 79 D S VUNCK

UNCLASSIFIED AFIT/GEP/PH/79D-12 NL

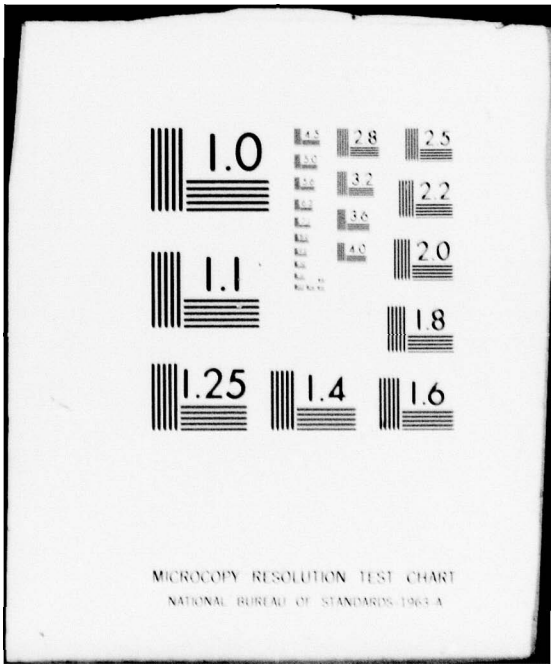
1.0
1.1
1.25
1.4
1.6
2.8
3.2
3.6
4.0
2.5
2.2
2.0
1.8
MICROCOPY RESOLUTION TEST CHART
NATIONAL BUREAU OF STANDARDS-1963-A

AFIT/GEP/PH/79D-12

EFFECTS OF SULFURHEXAFLOURIDE ON IONIZATION WAVES IN AN ARGON GLOW DISCHARGE

THESIS

AFIT/GEP/PH/79D-12 Darius S. Vunck
2nd Lt USAF

AFIT/GEP/PH/79D-12

(14)

(6) EFFECTS OF SULFURHEXAFLOURIDE ON IONIZATION WAVES IN AN ARGON GLOW DISCHARGE.

(9) Master's THESIS,

Presented to the Faculty of the School of Engineering
of the Air Force Institute of Technology
Air University
in Partial Fulfillment of the
Requirements for the Degree of
Master of Science

by

(10) Darius S. Vunck, B.S.
2nd Lt USAF
Graduate Engineering Physics

(12) 99

(11) Dec [redacted] 979

Approved for public release; distribution unlimited.

012 225

Preface

Interest in electronegative gases has grown recently as applications of such gases in electric discharge lasers, high power switching and electronics has increased. U.S. Air Force interest, in particular, has focused on the behavior and effects of electronegative gases in rare gas-halogen lasers. Such gases form negative ions which affect the dispersion properties of ionization waves inside an electric discharge and tend to make the discharge unstable. CO_2 electric discharge lasers for example can form O^- ions which can affect the operational performance of the laser. By using a glow discharge operated at low pressures and currents, this thesis will investigate the effect of negative ions, introduced in trace amounts, on the behavior of an Argon glow discharge.

The method used to analyze and measure the effects of negative ions is based on the artificial stimulation of ionization waves by voltage pulsing and current modulation recorded by Stirand space-time oscillograms.

Special thanks is given to Vivien Merchant and Peter Bletzinger for their help in getting sometimes balky instruments to behave as well as for providing helpful insights in analyzing photographic data.

Contents

List of Figures

List of Symbols

Symbol	
Ar	Argon
CO	Carbonmonoxide
SF_6	Sulfurhexaflouride
E	Electric Field
J_e	Electron Current Density
i	Current
n_e	Electron Number Density
n_+	Positive Ion Number Density
n_-	Negative Ion Number Density
n_a	Argon Number Density
n_s	SF_6 Number Density
n_c	CO Number Density
ν_u	Total Electron Energy Loss Collision Frequency
T_e	Electron Temperature
k_a	Attachment Rate
k_d	Detachment Rate
k_i	Ionization Rate
k_r^e	Electron-Ion Recombination Rate
k_r^i	Ion-Ion Recombination Rate
v	Electron Velocity
σ	Cross-sectional Area
SCCM	Standard Cubic Centimeters per Minute (1 cc of Nitrogen Gas at STP)

Abstract

Sulfurhexaflouride was added in varying trace amounts to a low pressure Argon glow discharge operated at 2.0 to 2.5 Torr and 1.0 to 30.0 mA. Using current modulation and voltage pulsing techniques with a space-time oscilloscope display, the dispersion of ionization waves was measured as a function of sulfurhexaflouride added.

It was determined that the addition of sulfurhexaflouride reduced the dispersion of the ionization waves and was directing the waves from a backward to forward wave nature with the group velocity traveling from cathode to anode. An actual change from backward to forward wave was not observed since the sulfurhexaflouride induces a breakdown of single mode wave oscillations when added in amounts equaling several percent of the gas mixture.

Carbonmonoxide gas was also introduced to the discharge and it was observed that the carbonmonoxide acted to reverse the effects of sulfurhexaflouride on the dispersion behavior of the ionization waves.

EFFECTS OF SULFURHEXAFLOURIDE ON IONIZATION WAVES IN AN ARGON GLOW DISCHARGE

I. Introduction

Electronegative gases such as sulfurhexaflouride, SF_6, possess a natural affinity for electrons. This property makes such gases valuable as insulators. For example, electrons that develop in arcs or short circuits can be captured by electronegative gas molecules. In recent years, U.S. Air Force interest has grown in electronegative gases for applications in high power switching and rare gas halogen lasers. To investigate the properties of electronegative gases in a plasma, glow discharges can be used.

A glow discharge is the partial ionization of a gas mixture between two oppositely charged electrodes. The glow is produced as ionized molecules recapture lost electrons. The light is, therefore quantized according to the energy levels of the gas. The ionizing mechanism is principally due to inelastic collisions between gas molecules and free electrons. Common applications of glow discharges can be found in neon lights and signs.

In this thesis, a glow discharge will be used to generate a plasma environment in which to study SF_6 gas. Trace amounts of the SF_6 gas will be introduced into the positive column of an electropositive glow discharge. To better understand the mechanisms and characteristics of glow discharges, a brief description will be given.

The Glow Discharge

The glow discharge consists of eight discrete regions. Each region will be detailed in order of occurrence following the cathode. The first region is called the Aston Dark Space. Here, electrons produced by positive ions striking the cathode and through ionized molecules are accelerated toward the anode. As the electrons accelerate, sufficient energy is gained to excite the gas molecules which then give off a bright glow during de-excitation. This region has consequently been named the Cathode Glow. As the electrons are further accelerated, inelastic collisions with gas molecules result in ionization. This region is consequently "dark" from the reduction of de-excitation and has been named the Cathode Fall or Cathode Dark Space. This region is further distinguished by a large drop in the electric field across the discharge. With electron energy reduced by ionizing collisions, excitation of gas molecules becomes evident again. In addition, electrons slowed

through inelastic collisions are recombined with positive ions. The de-excitation and recombination activity results in the release of light so this region has been named the Negative Glow.

With the reduction in electron energy, and ionization, excitation of gas molecules is reduced. The result is a dark region called the Faraday Dark Space which is easily observed in glow discharges.

The motion of the electrons during their passage through the above mentioned regions is changed so that it becomes randomized and can be approximated by a Maxwellian distribution. This is evident by moving the cathode relative to the discharge. The regions described above move with the cathode indicating a beam-like motion of the electrons while the regions following are not affected (Ref. 5:218).

Although it is the positive column of the glow discharge that is of interest for this thesis, this region is not essential to the discharge and can be eliminated through sufficient shortening of the discharge tube. The reason for the value of the positive column is that it represents a uniform and weakly ionized plasma. Within the positive column, the charges are balanced and represent approximately one part in a million of the particle population. In addition, the temperature (for both neutrals and electrons), electric field, and electron/ion density are

uniform across the region. The length of the positive column has no impact on any of these parameters. For this thesis, the tube length will be such that the positive column is the predominant feature of the glow discharge.

The glow in this region is caused by inelastic collisions both ionizing and exciting the neutral molecules and recombination of ions and electrons. The rate of ionization is balanced by recombination and leakage of electrons and ions from the region.

Following the positive column, the electrons begin to accelerate toward the anode. Insufficient energy is attained, however, to excite or ionize neutral molecules and this region has hence been named the Anode Dark Space. With further acceleration, the electrons begin to excite and ionize the gas molecules. This occurs very close to the Anode and is called the Anode Glow.

In most glow discharges, only few of the above features are visible. In most cases, the Cathode Glow, Faraday Dark Space, Positive Column and Anode Glow are the only visibile regions. Fig. 1 details the regions described above.

Striations

Within the positive column, waves of various types can be detected through optical and other techniques. These waves occur over a large range of frequencies and

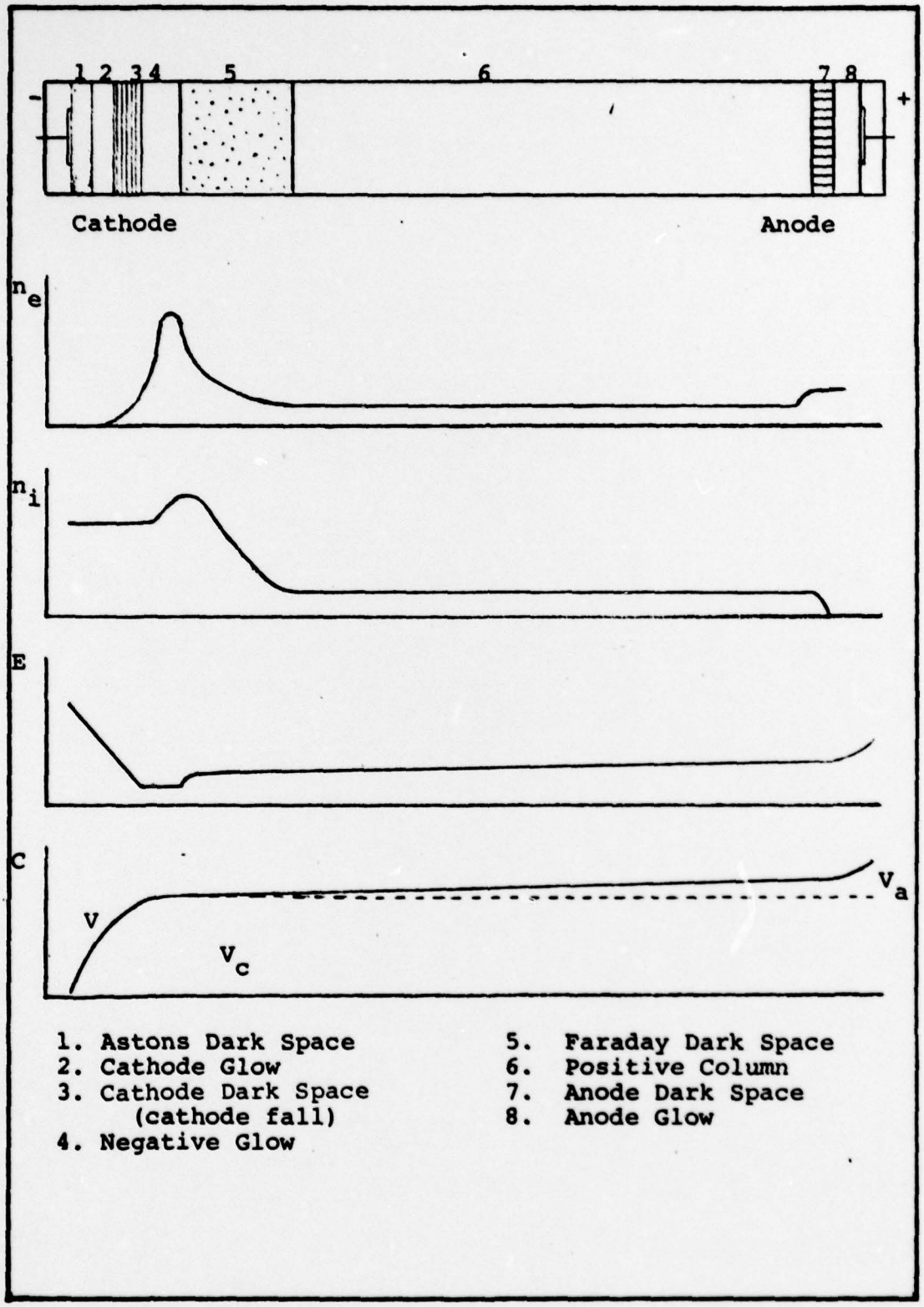

Fig. 1. The Glow Discharge

represent different physical phenomena (Ref. 8:66). For glow discharges with ambipolar diffusion, the waves detected within the positive column are called moving striation waves. They represent modulations in the electron number density, n_e, and temperature, T_e. The frequency for these waves ranges from 10^3 to 10^5 Hz.

Physically, striation waves are perturbations in the physical parameters of the positive column which affect the ionization rate. Striation waves, therefore, represent an inhomogeneity within the glow discharge.

Gradients in the electron/ion number density are the cause of self-excited striation waves. A small perturbation in the number density of electrons and ions will diminish but at different rates since the electrons have a higher mobility. This results in a separation of charge which affects the local electric field. Since the temperature is in turn affected by the field change, the temperature dependent rate of ionization is also altered. See Fig. 2. The locally altered ionization rate produces another gradient in n_e and n_i which repeats the above process. In this manner, the perturbations will propagate across the tube.

If human eyes were fast enough, the striation waves could be seen as moving vertical bars of light in the discharge tube. Fig. 3 shows how striations would appear if visible to the human eye. The diagram

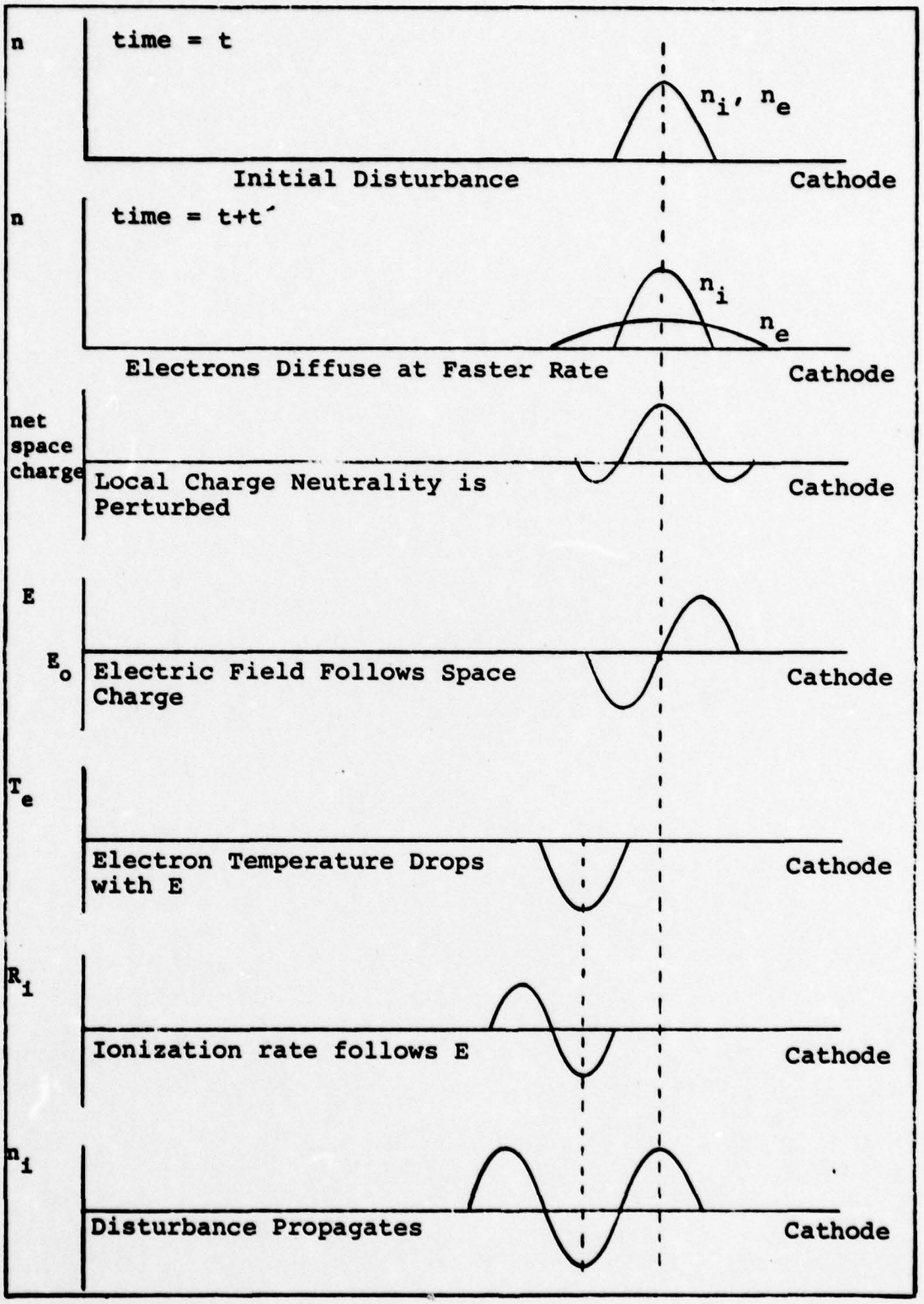

Fig. 2. Striation Development

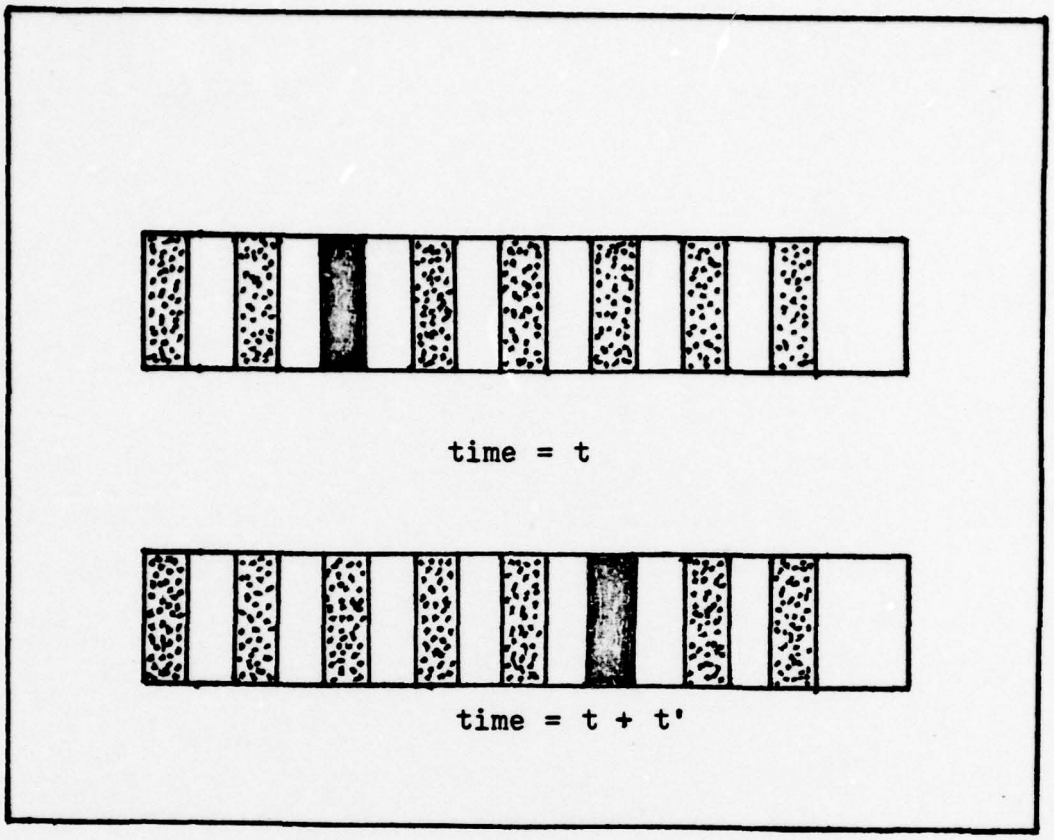

Fig. 3. Physical Appearance of Striations

illustrates the appearance of striations as generated by current modulation. The darkened bar shows how the striations move with time.

The appearance of striations generated by voltage pulsing is slightly different. Fig. 4 shows this difference. A good description of the physical appearance of voltage pulsed striations would be a horizontal, rotating barber pole moving down the discharge tube. Depending on the direction of rotation, the light bars in the "pole"

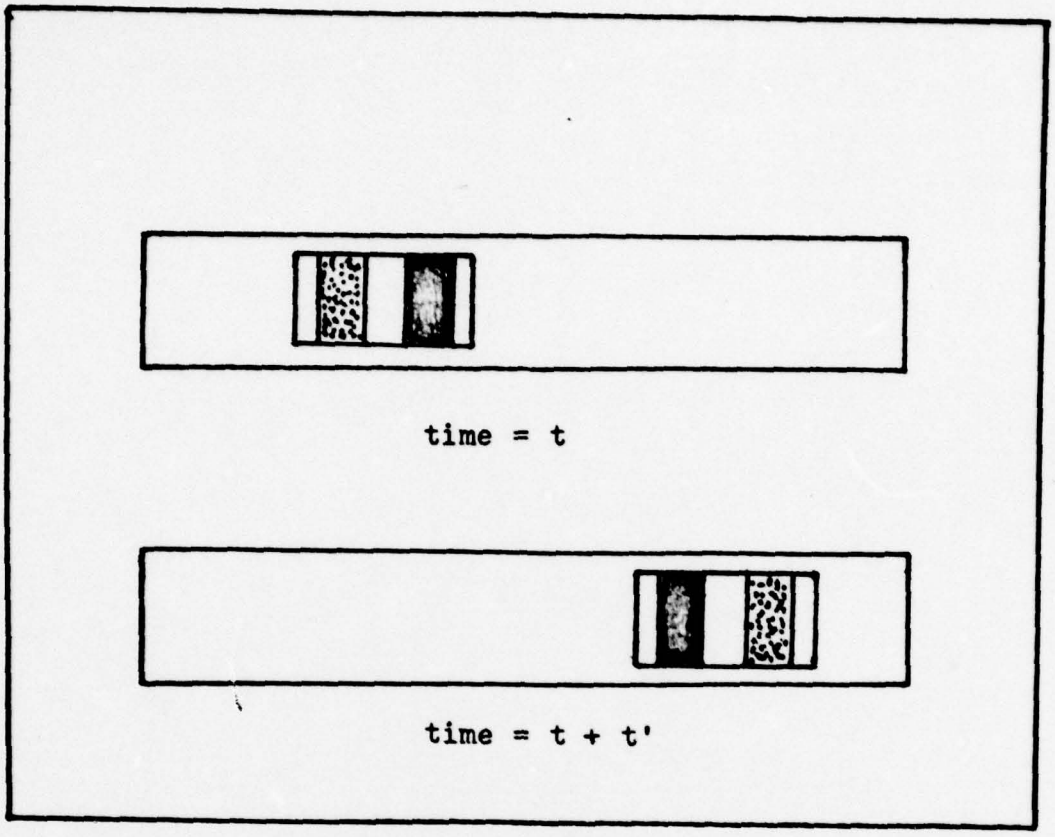

Fig. 4. Voltage Pulsed Striations

could be travelling in the same or opposite direction to the pole.

Physically, the light bars represent the phase velocity of the striations when measured against time. The voltage pulsed striations are the superposition of several striations of different frequencies. The "pole," therefore, gives the group velocity when measured against time.

Striation waves are classified into four types. If the phase velocity proceeds fron anode to cathode, the

wave is classified as a positive wave. The opposite of this is classified as a negative wave. An additional categorization is attached depending on the direction of the group velocity. A positive wave whose group velocity travels in the same direction as the phase velocity is called a positive-forward wave. When group and phase velocities are in opposite directions, the wave is called a positive-backward wave. The same procedure is used in classifying negative waves. In the case of electropositive gas discharges, backward waves are observed (Ref. 8:68-75).

Discharge Mechanisms

In this thesis, a glow discharge using Argon gas as the buffer will be investigated. The tube is of an open flow design and will be pressurized to between two and three Torr. Using the equation

$$PV = Nk_BT \qquad (1)$$

an estimate of the number density can be made with P=2.5 Torr, T=300°k and with $k_B=1.38\text{x}10^{-16}$ dyne-cm/°k. A value of $n=8.05\text{x}10^{16}$ molecules/cm^3 is obtained. With approximately 0.0001 percent ionization, n_e and n_i are about $8.05\text{x}10^{10}$/cm. For the glow discharge involving only Argon gas, three processes must be balanced: ionization, recombination, and diffusion. With the addition of trace

amounts of SF_6, gas, attachment must also be considered. The equations involved are:

$$\frac{dn_e}{dt} = k_i n_e n_a + k_d n_- n_c - k_r^e n_e n_i - k_a n_e n_s \qquad (2)$$

$$\frac{dn_-}{dt} = k_a n_s n_e - k_r^i n_+ n_- - k_d n_- n_c \qquad (3)$$

In the above equations, k_i is the rate of ionization, k_d is the detachment, k_r is the rate of recombination, k_a is the attachment coefficient, n_- is the negative ion number density, n_+ is the positive ion number density, while n_s and n_c are the SF_6 and CO densities respectively. A solution of these equations gives the dispersion characteristics of the glow discharge.

The rate of ionization, k_i, can be written as

$$k_i = n_a \sigma V_e \qquad (4)$$

where σ is the cross-sectional area of Argon and V_e is the velocity of the electrons.

These equations will be further developed in the theory section.

The glow discharge represents the physical solution to the above equations. The processes are kept in balance according to the voltage applied to the electrodes.

Scope of Research

For this thesis, striation waves will be observed with optical methods described later. The dispersion of the striation waves will be measured as a means to determine their stability in a glow discharge containing trace amounts of SF_6 and CO gas. The techniques are similar to those developed by Stirand et al. (Ref. 25:481) and further developed by Garscadden and Bletzinger (Ref. 7:149).

Previous Work

Investigations of glow discharges first began during the late 1800s. In the late 1850s, Geisler developed methods for building discharge tubes such as used in this thesis. Early investigators such as Thomson and Aston, Crookes, and Hertz in the late Nineteenth Century and Faraday and others in this century performed pioneering work and are remembered in some cases by having their names associated with glow discharge phenomena. Not until relatively late, however, were the physical mechanisms associated with the discharge explained.

In the early 1960s, work by Garscadden, Lee and Bletzinger and by Pekarek and Krejci provided an initial understanding of the discharge processes. Latter efforts involving the same researchers and others resulted in more refined and accurate theoretical models showing much better agreement with experimental results. The scope of

the theories also grew deeper encompassing the effects of metastables and negative ions (Refs. 1, 2, 12, 19, 22).

The effects of negative ions in particular have been given great attention in recent years and accurate theoretical models now exist which describe the effects of negative ions on a glow discharge particularly in regards to the stability of the ionization waves (Ref. 17).

Experiments are now being conducted throughout the world particularly in Russia, Japan, and eastern Europe in response to new areas of applications of electronegative gases in electronics and lasers.

Statement of Problem

In recent years, interest has grown in electronegative gas discharges. The object of this study is to conduct experiments using a glow discharge to determine the instabilities associated with the presence of trace amounts of SF_6 gas in an Argon gas discharge at low pressures and currents. In addition, this study will examine the results of adding CO to an Ar/SF_6 mixture to determine if the effects of the SF_6 can be reduced.

The method of investigation will be by the photomultiplier correlation technique (Ref. 25:1481). Data yielded by this technique provides information on the dispersion characteristics of the ionization or striation waves present in the positive column by applying

analytical models developed by Pekarek (Ref. 12:866) and Stirand et al. (Ref. 25:1481-1484).

II. Theory

Numerous theoretical solutions to the behavior and stability of glow discharges have been made during the last fifteen years. Early works covered simple discharges without considering metastables or negative ions (Ref. 14: 567-581). These two features have been considered in later works (Refs. 2, 18) and today many theoretical models describing complex glow discharges are available.

Nighan and Wiegand (Ref. 18) have done considerable work in glow discharges containing negative ions. Using results developed by Haas (Ref. 9), they derived stability models for discharges affected by negative ions as well as a detaching species.

The results obtained by Nighan and Wiegand can be easily tailored to model the conditions presented for the glow discharge in this thesis. An outline of their development along with changes to fit the discharge conditions for this thesis will be presented.

Three basic equations are used to develop an expression describing the criterion for ionization instability: the electron continuity equation, the negative ion continuity equation, and the electron energy equation.

$$\frac{dn_e}{dt} = k_i n_e n_a - k_r^e n_e n_+ - k_a n_e n_s + k_d n_- n_c \qquad (5)$$

$$\frac{dn_i}{dt} = k_a n_e n_s - k_d n_- n_c - k_r^i n_- n_+ \qquad (6)$$

$$\frac{d}{dt}(3/2\, n_e k T_e) = J_e E - n_e n_a \left(\frac{\nu_u}{n_a}\right) K T_e \qquad (7)$$

Equations 5, 6, and 7 are tailored to this thesis. The terms involved are the number densities for electrons, n_e, negative ions, n_-, positive ions, n_+, Argon, n_a, SF_6, n_s, and CO, n_c. The rate expressions are for ionization, k_i, attachment, k_a, detachment, k_d, electron-ion recombination, k_r^e, and ion-ion recombination, k_r^i. In equation 7, k is Boltzman's constant, T_e is the electron temperature (in eV), E is the electric field, J_e is the electron current density, and ν_u is the total electron energy loss collision frequency. The equation for positive ion continuity is ignored through charge neutrality:

$$n_+ = n_- + n_e \qquad (8)$$

The rate expressions are useful across a range of T_e provided that

$$T_e(E/N) = 2/3\,\bar{u} = 2/3 \int_0^\infty u^{3/2} f(u, E/n)\, du \qquad (9)$$

where u is the electron energy in eV, and f is the electron energy distribution function.

Perturbations are now introduced by rewriting several terms as below.

$$n_e \rightarrow n_e + \tilde{n}_e \tag{10}$$

$$n_- \rightarrow n_- + \tilde{n}_- \tag{11}$$

$$E \rightarrow E + \tilde{E} \tag{12}$$

$$J \rightarrow J + \tilde{J} \tag{13}$$

$$T_e \rightarrow T_e + \tilde{T}_e \tag{14}$$

$$\nu_u \rightarrow \nu_u + \tilde{\nu}_u \tag{15}$$

In the case of E, J, T_e and ν_u, the perturbed parts, $\tilde{x}$, are developed as shown below.

The definition for a derivation is:

$$\frac{dM}{dN} = \frac{M(N+\Delta N) - M(N)}{\Delta N} \tag{16}$$

Equation 17 can be rewritten as:

$$M(N+\Delta N) = M(N) + \Delta N \frac{dM}{dN} \tag{17}$$

The last term of equation 18 is related to $\tilde{M}$. The <u>fractional</u> derivation of $\tilde{M}$ is

$$\hat{M} = \frac{N}{M} \frac{dM}{dN} = \frac{d \ln N}{d \ln M} \tag{18}$$

Using equation 7 and the above, $\tilde{T}_e$, $\tilde{E}$ and $\tilde{n}_e$ can be related. However, equation 7 is first changed by deleting the time derivative. This is possible because changes in the electron energy distribution is instantaneous compared to changes in the charged particle densities. As developed by Haas, the result is

$$\frac{\tilde{T}_e}{T_e} = \left(\frac{-\cos^2\phi}{1+\hat{\nu}_u-\hat{\nu}_m\cos 2\phi}\right)\frac{\tilde{n}_e}{n_e} = \left(\frac{-2\cos^2\phi}{\hat{\nu}_u'}\right)\frac{\tilde{n}_e}{n_e} \qquad (19)$$

where ϕ is the angle between the wave propagation vector and the electron current, J_e, and ν_m is the electron momentum transfer collision frequency.

To develop the expression giving the instability criterion, equations 5, 6, and 7 must be rewritten using the substitutions given in equations 11 through 16. The results are shown below.

$$\begin{aligned}\frac{d\tilde{n}_e}{dt} &= k_i\tilde{n}_e n_a + \tilde{k}_i n_e n_a - k_r^e\tilde{n}_e n_+ - k_r^e n_e\tilde{n}_+ - \tilde{k}_r^e n_e n_+ \\ &\quad - k_a\tilde{n}_e n_s - \tilde{k}_a n_e n_s + k_d\tilde{n}_- n_c + \tilde{k}_d n_- n_c \\ &\quad +(k_i n_e n_a - k_r^e n_e n_+ - k_a n_e n_s + k_d n_- n_c) \qquad (20)\end{aligned}$$

Second order perturbations are ignored in the above development. An additional reduction is made by assuming steady state conditions which result in the elimination of the terms within the parentheses.

Performing the same development on 7 and 8 results in a set of linearized first order perturbation equations.

$$\frac{d\tilde{n}_e}{dt} = k_i \tilde{n}_e n_a + \tilde{k}_i n_e n_a - k_r^e \tilde{n}_e n_+ - k_r^e n_e \tilde{n}_+ - \tilde{k}_r^e n_e n_+ - k_a \tilde{n}_e n_s - \tilde{k}_a n_e n_s + k_d \tilde{n}_- n_c + \tilde{k}_d n_- n_c \quad (21)$$

$$\frac{dn_-}{dt} = k_a \tilde{n}_e n_s + \tilde{k}_a n_e n_s - k_d \tilde{n}_- n_c - \tilde{k}_d n_- n_c - k_r^i \tilde{n}_- n_+ - k_r^i n_- \tilde{n}_+ - \tilde{k}_r^i n_- n_+ \quad (22)$$

$$\frac{d}{dt}\left(3/2\,\tilde{n}_e kT_e + 3/2 n_e k\tilde{T}_e\right) = J_e \cdot \tilde{E} + \tilde{J}_e \cdot E - \tilde{n}_e n_a \left(\frac{\nu_u}{n_a}\right) kT_e - n_e n_a \left(\frac{\tilde{\nu}_u}{n_a}\right) kT_e - n_e n_a \left(\frac{\nu_u}{n_a}\right) k\tilde{T}_e \quad (23)$$

In the above equations, k_a, k_i, k_r^e, k_r^i, and k_d are perturbed as described earlier with respect to T_e. The perturbed parts of n_e, n_-, and n_+ take the form shown below.

$$\tilde{n}_e \rightarrow \tilde{n}_e\, e^{-i(\omega t - kx)} \quad (24)$$

$$\tilde{n}_- \rightarrow \tilde{n}_- e^{-i(\omega t - kx)} \quad (25)$$

$$\tilde{n}_+ \rightarrow \tilde{n}_+\, e^{-i(\omega t - kx)} \quad (26)$$

The form of the perturbations in the number densities relate to variations in space and time. ω is a complex term as shown below.

$$\omega = \omega_r + i\omega_i \tag{27}$$

The real part of ω when related to the unperturbed terms in the above equations will give the conditions under which ionization instabilities will grow or dampen. The imaginary part of ω will give the dispersion behavior of the plane waves represented by equations 24 through 26.

The time derivatives in equations 21 and 22 will result in two equations with ω. Equation 23 is treated as before eliminating the time derivative.

The result of the above actions results in a set of three linear equations containing ω and first order perturbation terms. In this set of three equations are three unknowns: $\tilde{n}_e$, $\tilde{n}_-$ and $\tilde{n}_+$. The equations are finally rearranged with all terms collected to one side.

Using equation 19 and placing the set of 3 linear equations into a 3x3 matrix, ω can be determined by solving for the determinant and setting it equal to zero. The result is a product consisting of a quadratic and a first order expression in ω. Only the quadratic is of interest since it alone is associated with negative ion production and loss.

Using the expression developed by Nighan and Wiegand and adjusting for the particular conditions described earlier, the result is:

$$2R_e(i\omega) = -b \pm 1/2\ (b^2-4ac)^{\frac{1}{2}} \tag{28}$$

where

$$b = n_a k_i \hat{k}_i - \left(\frac{2\cos^2\phi}{\hat{\nu}_u'}\right)\left(1 - \frac{k_a \hat{k}_a}{k_i \hat{k}_k}\right) + \left(\frac{n_e}{n_+} k_r^e + \frac{n_-}{n_e} n_a k_d + \frac{n_a}{n_+} n_+ k_r^i + \frac{n_e}{n_-} n_a k_a\right) \quad (29)$$

$$a = 1 \quad (30)$$

and

$$c = n_a k_i \hat{k}_i \left(\frac{2\cos^2\phi}{\hat{\nu}_u'}\right)\left[\left(\frac{n_a}{n_+} n_+ k_r^i + \frac{n_e}{n_-} n_a k_a\right) - \left((1 + \frac{n_-}{n_+})\ n_+ k_r^i + \frac{n_e}{n_+} n_+ k_r^e\right)\ \frac{k_a \hat{k}_a}{k_i \hat{k}_i}\right] + \left[\frac{n_e}{n_a} n_a k_a n_+ k_r^e + \frac{n_a}{n_e} n_+ k_r^i n_a k_d\right] \quad (31)$$

The condition for instability is $b < 0$.

$$\left[\left(\frac{-2\cos^2\phi}{\hat{\nu}_u'}\right)\left(1 - \frac{k_a \hat{k}_a}{k_i \hat{k}_i}\right) n_a \hat{k}_i\right] - \left(\frac{n_e}{n_+} n{+}k_r^e + \frac{n_-}{n_e} n_a k_d + \frac{n_-}{n_+} n{+}k_r^i + \frac{n_e}{n_-} n_a k_a\right) > 0 \quad (32)$$

Physically, the first part of equation 32 describes the changes in the production and loss processes for electrons as a function of changes in T_e. The second part of

equation 32 links together the perturbations in electron and negative ion densities with the stabilizing processes of electron-ion recombination and negative ion detachment. All the terms of the second part in equation 32 are positive in an overall negative term with the minus sign in front. For the condition in equation 32 to be met, therefore, requires that the bracked terms be positive overall. Since $\hat{\nu}_u'$ is almost always positive this means that

$$\frac{k_a \hat{k}_a}{k_i \hat{k}_i} > 1 \qquad (33)$$

is necessary for ionization instability.

For self-sustained discharges, such as used for this thesis, the negative ion density must approximate the electron density for the processes affecting both to couple. Such coupling would then lead to attachment induced ionization instability. In the case where $n_- < n_e$ caused either through strong detachment or by mixing in extremely small amounts of electronegative gas, then no coupling can occur. On the other hand, if $n_- > n_e$, then for instability to occur, the condition

$$\frac{k_a \hat{k}_a}{k_i \hat{k}_i} + \frac{\hat{k}_a}{\hat{k}_i} > 1 \qquad (34)$$

must hold. However, the ionization rate is almost always more dependent on T_e than the attachment rate. So for

conditions where $n_- > n_e$ there will be no attachment induced ionization instability. Since the equipment used in this experiment is too inaccurate to flow SF_6 at parts per million with respect to the flow of Argon, the condition just described will be approximated.

Since striations are related to instabilities linked to the ionization process (Ref. 18:15), it should be expected that striations should weaken with increasing concentrations of SF_6 and return with further additions of CO.

The equations developed by Nighan and Wiegand, although straightforward, require considerable algebraic manipulations before reducing to their final form. The result, however, is a fully developed model containing all the processes and elements within the glow discharge. Simpler models can be developed (see Appendix A) but they are not as extensive in detail.

The operating conditions for this thesis have been mentioned earlier. The result was that n_e would be approximately $8 \times 10^{10}/cm^3$. The current for the discharge is approximately 10 mA. Using the equation

$$i = n_e q v A \tag{35}$$

where i is the current, q is the charge per electron, and A is the cross-sectional area of the discharge tube, the velocity of the electrons, v, can be determined. With

$A = \pi cm^2$, and $q = 1.6x10^{-19}c$, v is determined as shown below.

$$v = \frac{i}{n_e qA} \tag{36}$$

$$v = \frac{0.01\ c/s}{(8x10^{10}/cm^3)(1.6x10^{-19}c)(\pi cm^2)}$$

$$= 2.5 \times 10^5\ cm/s$$

The energy of the electrons can now be determined using the equation

$$v = 6.7x10^7\ (T_e)^{\frac{1}{2}}\ cm/s \tag{37}$$

where T_e is in electron volts (eV).

$$\left[\frac{2.5x10^5\ cm/s}{6.7x10^7\ cm/s}\right]^2 = T_e$$

so $$T_e = 1.4x10^{-5}\ eV$$

The energy of the electrons falls within the range of greatest cross-section for attachment in SF_6 (Ref. 3:611). The attachment rate should, therefore, be high for the discharge in this thesis, and the effects of SF_6 will then be quite noticeable even in very small trace amounts.

III. Equipment

Functional Description

In this experiment, Argon, SF_6, and CO gas are required to flow separately at varied and measured rates into a mixing manifold. The combined gases then continue into a discharge tube where they are excited and ionized by an electric field generated by two oppositely charged electrodes at either end of the discharge tube. While in the tube, the gases are measured for pressure and floures-cence. In addition, the current and voltage across the electrodes are also measured. The gases then continue to flow out the tube and are finally vented out through an exhaust system.

In the following text, the equipment devised to meet the above requirements will be described and illus-trated in four sections. Each section will detail the equipment used in solving the listed requirements.

Discharge Network

The discharge network entails all the equipment needed to establish and maintain a glow discharge. A schematic of the network is shown in Fig. 5. Included are the discharge tube, vacuum pump, vacuum ballast tank, mass

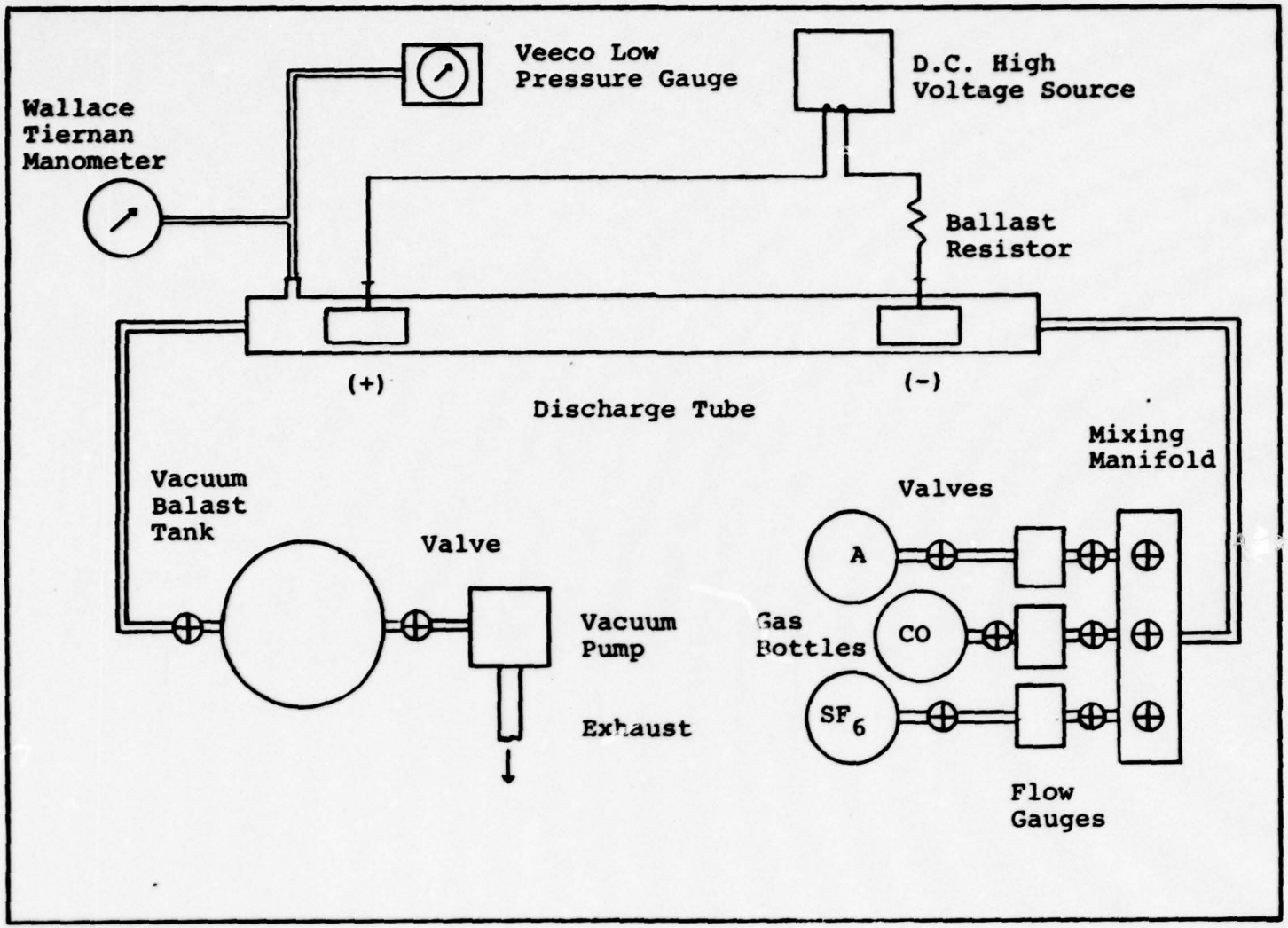

Fig. 5. Discharge Network

flow meters, gas mixing manifold, DC voltage supply, and pressure gauges.

The discharge tube is an open end pyrex tube two cm in diameter. The electrodes are made of Kovar and are spaced 50 cm apart. Both electrodes are hollow cylinders of identical size and may substitute for one another. A port is located behind the electrode serving as anode. The design is illustrated in Fig. 6 below.

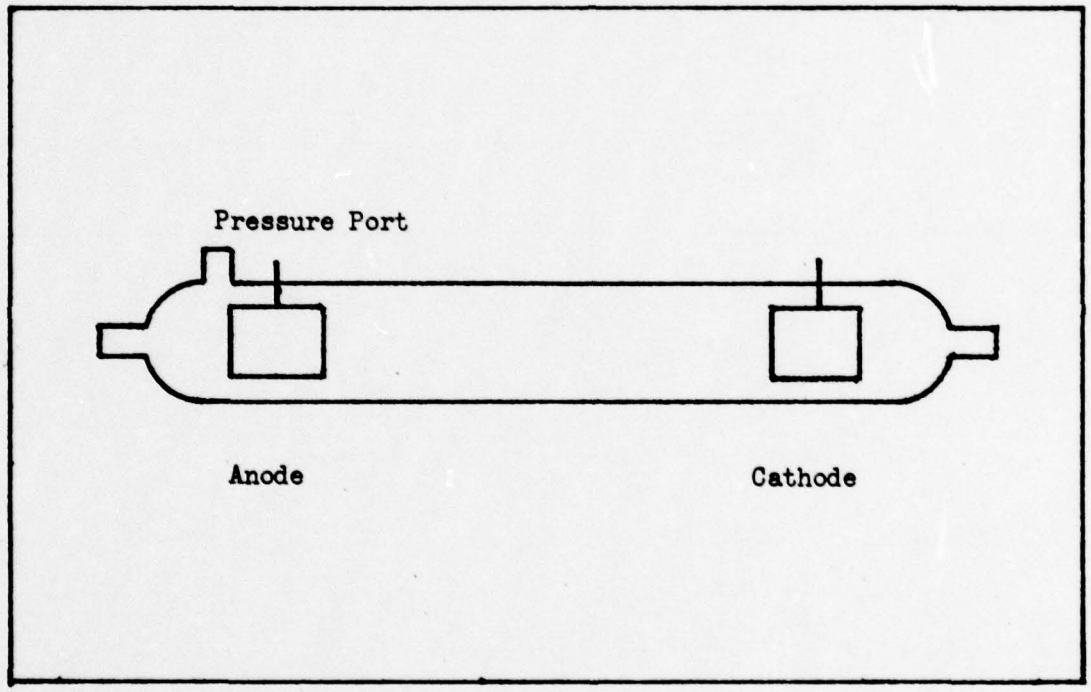

Fig. 6. Discharge Tube

The vacuum pump is a simple mechanical engine equipped with a valve to seal the vacuum after the engine is turned off. The pump is electrically powered and can be left operational for many days.

The vacuum ballast tank is a large cylindrical steel drum. It is equipped with entrance and exit ports designed for O-ring sealed clamps. The large volume of the tank provides a ballast against the effects of small leaks or sudden pressure changes.

Two types of pressure gauge are used in the network. A Wallace-Tiernan Type FA-160 absolute pressure indicator is used for pressures greater than one Torr. The gauge has a range of 0.1 to 20 Torr. A Veeco thermocouple gauge is used for pressures below one Torr. The range of the Veeco is 0 to 1,000 microns of Mercury.

A Gregory-King Electronics three kilowatt power supply provides the DC potential to the discharge tubes. The voltage is regulated and will not change once set regardness of discharge current. A nine kΩ ballast resistor is placed in series with the voltage source to prevent arcing in the discharge.

Two Hastings Mass Flowmeters are used to record the flow of the Argon and SF_6 gas. The meters are linear and calibrated for Nitrogen. A simple conversion constant permits use of other gases (1.43 for Argon and 0.27 for SF_6). The meters record flow in standard cubic centimeters per minute (SCCM).

Striation Driver

Striation waves can be driven by applying current modulation on the glow discharge. The driving system used in this thesis is a Hewlett-Packard Model 3300A Function Generator connected in series with a high voltage transistor and operational amplifier.

The function generator provides an AC voltage with manually adjustable frequency. The operational amplifier impresses the AC signal on an internal DC signal set by an adjustable bias control. The combined signal is then applied to the base lead of the transistor. The collector lead is connected to the cathode and the emitter to ground. The arrangement is shown in Fig. 7.

Measuring Equipment

The basic technique in analyzing striation waves for this thesis will follow the methods developed by Stirand et al. This will be discussed in detail in the measurement technique section. The equipment used consists of an oscilloscope capable of brightness modulation, a photomultiplier, a linear amplifier, and slide wire. The equipment arrangement is illustrated in Fig. 8.

The photomultiplier is an Orion Model D-21-20 equipped with a lens positioned to provide a unit magnification of the object onto the photomultiplier slit. The signal from the photomultiplier is linearly amplified

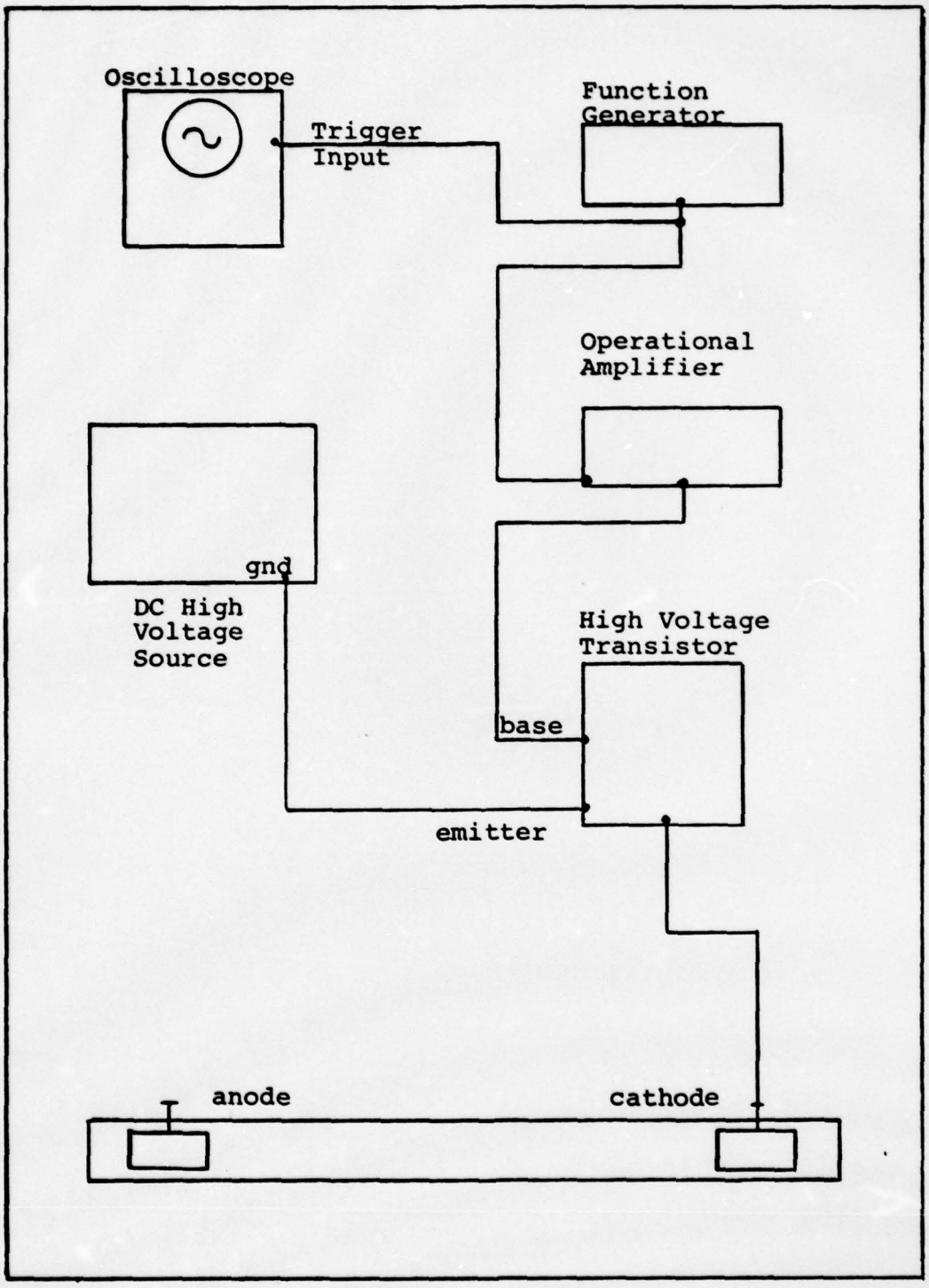

Fig. 7. Driver Schematic

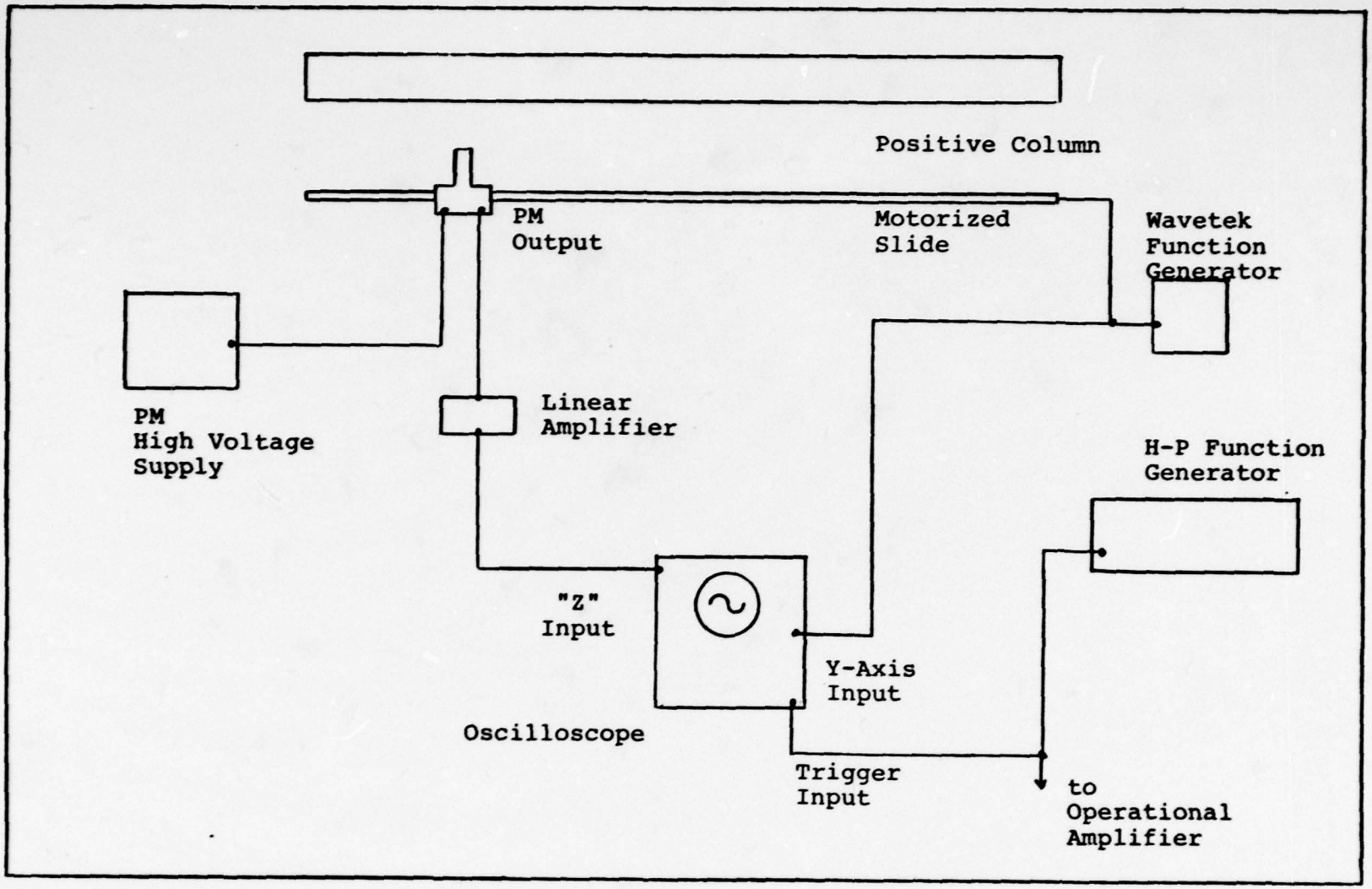

Fig. 8 . Measuring Equipment

and used to brightness modulate a Tektronix Model 502 Dual Trace Oscilloscope. The oscilloscope trace is interrupted whenever a signal of greater than 25 volts is received from the amplifier.

A motorized slide is used to sweep the photomultiplier across the length of the positive column. A Wavetak Model 144 High Frequency Sweep Generator producing a triangle pulse current is employed to provide the voltage sweep powering the slide. In addition, the oscilloscope trace y-axis is also driven by the Wavetak resulting in a linkage between photomultiplier position and trace height along the y-axis of the oscilloscope.

The scope signal is triggered by the H-P function generator also used to drive the striation waves. The resulting display presents a space-time picture from which phase velocity, wavelength and frequency can be obtained.

A permanent record of the oscilloscope trace is made with a Polaroid Land camera attached directly to the oscilloscope screen. The camera is equipped with a Tektronix-Simpson 85 mm lens series 125 set to f/4.5 and manual shutter control. Polaroid Type 47 high speed film is used. The film has an 3000 ASA rating which permits screen brightness to be lowered giving the trace more contrast. Fig. 9 is a representation of a typical extended exposure trace.

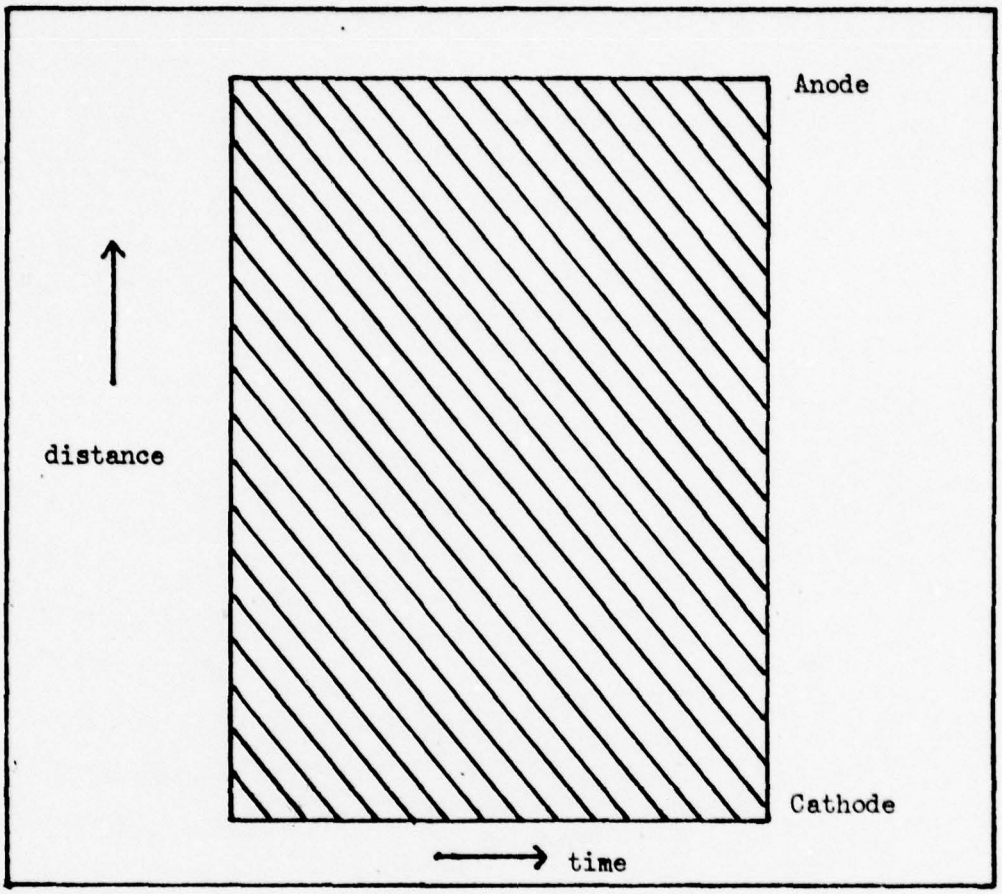

Fig. 9. Representative Photograph

In addition to the above instruments, a milliameter is connected across the discharge tube to provide a measure of the discharge current. Also, a digital multimeter set to DC voltage is connected across the base and emitter leads to the transistor. Transistor voltage will vary with discharge current and may range up to 40.0 volts.

Voltage Pulser

The AC driving equipment detailed earlier does not provide all the desired information on the striation wave propagation. Specifically, group velocity and the direction of propagation are not shown. To do this, a pulser network is built as shown in Fig. 10. The pulser applies a high voltage impulse of many frequencies to a local area within the positive column. This generates a single wave packet which then propagates along the tube. The direction of the propagation and group velocity can be measured directly using the same measuring equipment described earlier.

Pulser Network

The pulser network consists of a high voltage Thyratron, a Wavetek Function Generator and a voltage loop. The Thyratron can apply a voltage pulse from one to fifteen kV in 50ns. The trigger for the Thyratron is a square pulse signal from the Wavetek Function Generator which simultaneously serves to trigger the oscilloscope. The Thyratron can be set up to a maximum of five Hz.

The output from the Thyratron is sent to a loop of copper wire. The loop does not form a complete circle but instead has a gap which effectively makes the loop into a capacitor. The loop is placed one cm from the

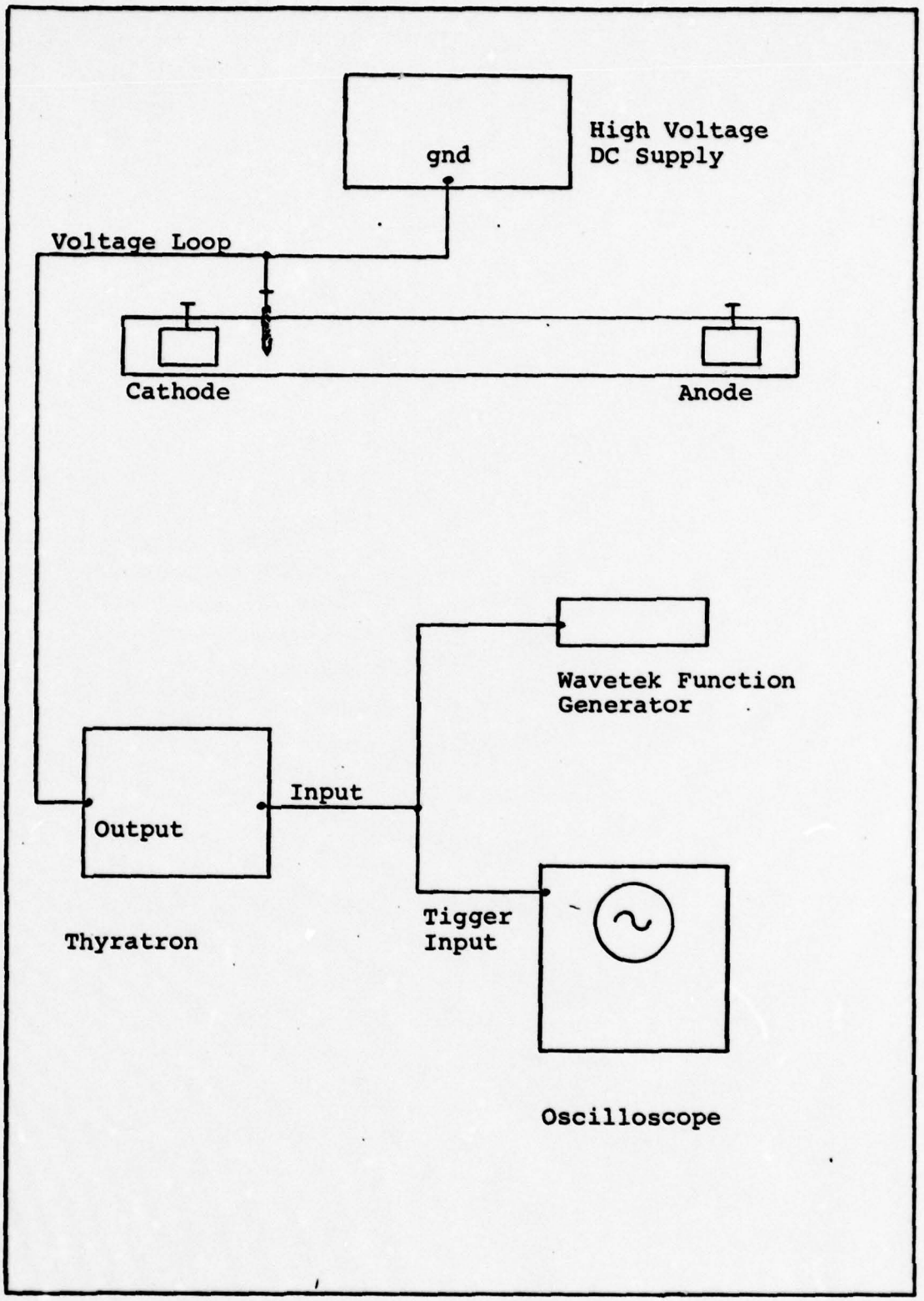

Fig. 10. Pulser Network

cathode in this thesis. Another lead from the output is grounded back into the DC supply ground.

The voltage loop is securely fastened with insulated clamps to insure no accidental grounding directly from the loop.

IV. Measurement Technique

Space-time oscillograms are a powerful tool which permit real time measurements of striation waves. Parameters such as wavelength, frequency, phase velocity, and group velocity can be measured using this technique. With these data, dispersion plots of phase velocity versus frequency or angular frequency versus wave number can be drawn.

Space-Time Correlation

Striation waves are highly stable and repetitive over time. This permits a long sampling period (in this experiment approximately 30 seconds) across the positive column. During the sampling period, many thousands of individual striation waves will have passed through the positive column. Yet each wave matches the positional-time profile of the previous wave so closely that differences are irresolvable with the equipment used in this experiment.

The repeatability of the striation waves is what permits space-time oscillograms to be constructed.

Procedure

The procedure of constructing a space-time oscillogram is detailed below.

It is possible to control the vertical position of an oscilloscope trace with a controlled input voltage. This same voltage is used to drive a photomultiplier across the length of the positive column. Therefore, a given point on the vertical axis of the oscilloscope corresponds to some position along the positive column. The horizontal axis of the oscilloscope is based on time. For example, with a time base set to 0.5 ms on the oscilloscope controls, the horizontal axis represents a period of 5 ms during which a photomultiplier is observing a single point of the positive column. During this time, a number of striations will pass the photomultiplier. The striations are driven by methods described elsewhere and the oscilloscope is triggered to commence a trace in synchronization with the driving system.

For a given point on the vertical axis, the oscilloscope will show a steady, unvarying sinusoidal wave. By connecting the photomultiplier output into the brightness modulation control of the oscilloscope, the trace will become a flat "dashed" line. This trace represents a sweep across the time axis interrupted at points when the photomultiplier sees a passing wave. After the photomultiplier shifts position (shifting the oscilloscope trace on the vertical axis), the process is repeated.

The shift in photomultiplier position means that the striations require more less time to reach the

photomultiplier. This results in the dashed line being shifted by some amount on the time axis. Fig. 11 shows a sequence illustrating the construction of a space-time oscillogram.

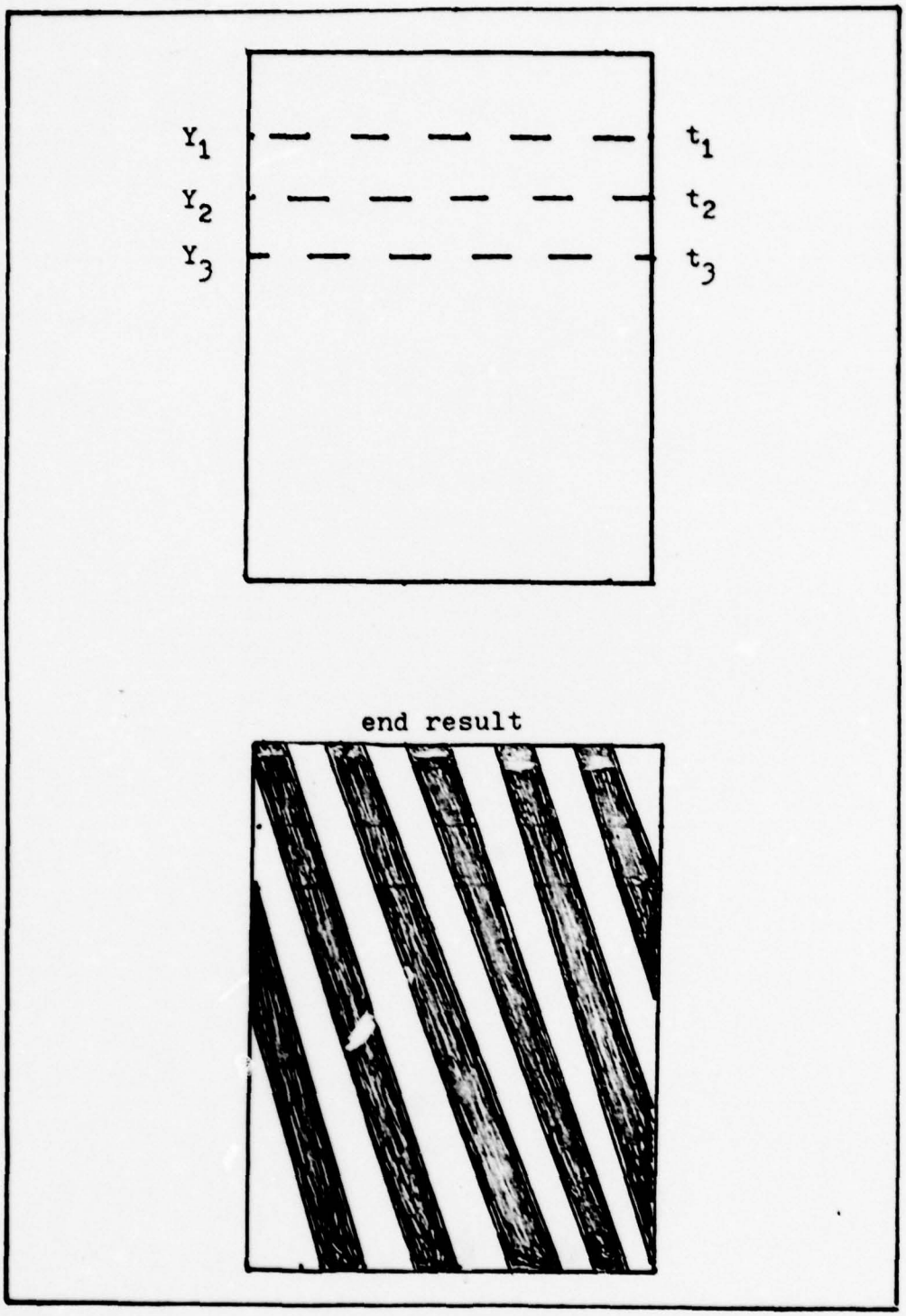

Fig. 11. Space-Time Photograph Construction

V. Procedures

Contained in this section is a detailed description of the procedures and methods used in operating the equipment described earlier, and in obtaining and recording data. The following text will determine the operations in the order they are performed.

Evacuation

In evacuating the discharge network, all but the valve separating the pump from the ballast tank are closed. the Vacuum pump and Veeco pressure gauge are then activated. The pump is allowed to operate continuously until data collection ends, and no data will be obtained until 24 hours after the pump is started.

Leak Test

At the end of the 24 hour pumping period, the valve to the ballast tank is closed and a time versus pressure record is made using the Veeco low pressure gauge. A pressure of 11 microns of Hg was found to be the minimum pressure possible, and a leak-up rate of three microns per minute was averaged over a two hour period. A non-linear pressure rise would indicate outgassing, but

continuous pumping insured no internal contamination. Following the leak test, the pump is restarted and the valve to the ballast tank reopened after the pump has evacuated itself.

Gas Introduction

The flowmeter connected to the Argon supply bottle is activated and the valve to the Argon regulator opened to permit 20 lbs pressure to the mixing manifold. The outer valve to the manifold is opened and the inner valve slowly opened via vernier control. The inner valve is allowed to continue opening until the desired pressure is reached as recorded by the pressure gauges. The flowmeter value is then recorded. Introduction of the SF_6 follows the same procedures except that the amount permitted to enter is insufficient to register on the pressure gauges and is, therefore, adjusted as desired by observing the effect of the gas on the discharge.

Discharge Establishment

The glow discharge is established by the use of a Tesla coil for initial sparking since the cold cathode arrangement requires a large sparking potential. The discharge tube DC supply is set at 800 V and the operational amplifier set to permit current flow through its adjustable bias control. The AC source for striation driving

need not be turned on but generally is since a variable resistor to the amplifier can prevent any leakage of signal from the driver. The discharge current and transistor voltage are measured using the ammeter and multimeter described earlier. The discharge current can be varied from 0 to 30 mA using the bias control on the amplifier. A current change will inversely affect the transistor voltage so readings from the current and volt meters are taken for each bias setting.

Data Collection

The two categories of data collected from the experiment are the current-voltage relationship, and the dispersion parameters. In addition, these data are taken for a range of pressures.

In taking the data for the current-voltage relationship, the transistor voltage is recorded from the multimeter as the discharge current is swept over a 30 mA range by the amplifier bias control. The current is incremented in 5 mA steps during the sweep. Care is taken to insure that the DC tube supply is constant during data collection since heavy electrical use by other experimenters can cause voltage variations.

Prior to actual dispersion measurements, a resonance map is made for Argon at various pressures and currents. This is done by connecting the photomultiplier

directly to the y-axis of the oscilloscope and varying the frequency control of the striation driver. The photomultiplier signal is triggered by the function generator signal and whenever the oscilloscope trace is synchronized this indicates a resonance frequency determined by the driver frequency control settings. A check is made to insure the striation trace is natural and not mode locked by the driver by reconverting to brightness modulation and checking to see if the oscilloscope trace resembles Fig. 9. If the lines are vertical then the trace is mode locked and does not represent a natural striation resonance. By using a small AC voltage, less than 50 mV, the effect of the driver is negligible.

Macroscopic observations of the glow tell whether a resonance zone is uniform. If the glow contains "bright spots," then the wave amplitude will vary considerably. These spots represent a slowdown in wave velocity and appear as stationary balls to the observer. See Fig. 12. A uniform glow appears diffuse and homogeneous. Wave amplitude as seen by the photomultiplier will be uniform in a homogeneous glow.

Dispersion measurements are made in resonance zones with uniform glows. The AC voltage is increased sufficiently to modulate the striation waves but short of mode locking the waves or changing the discharge to a nonuniform glow. A series of time lapse exposures are now

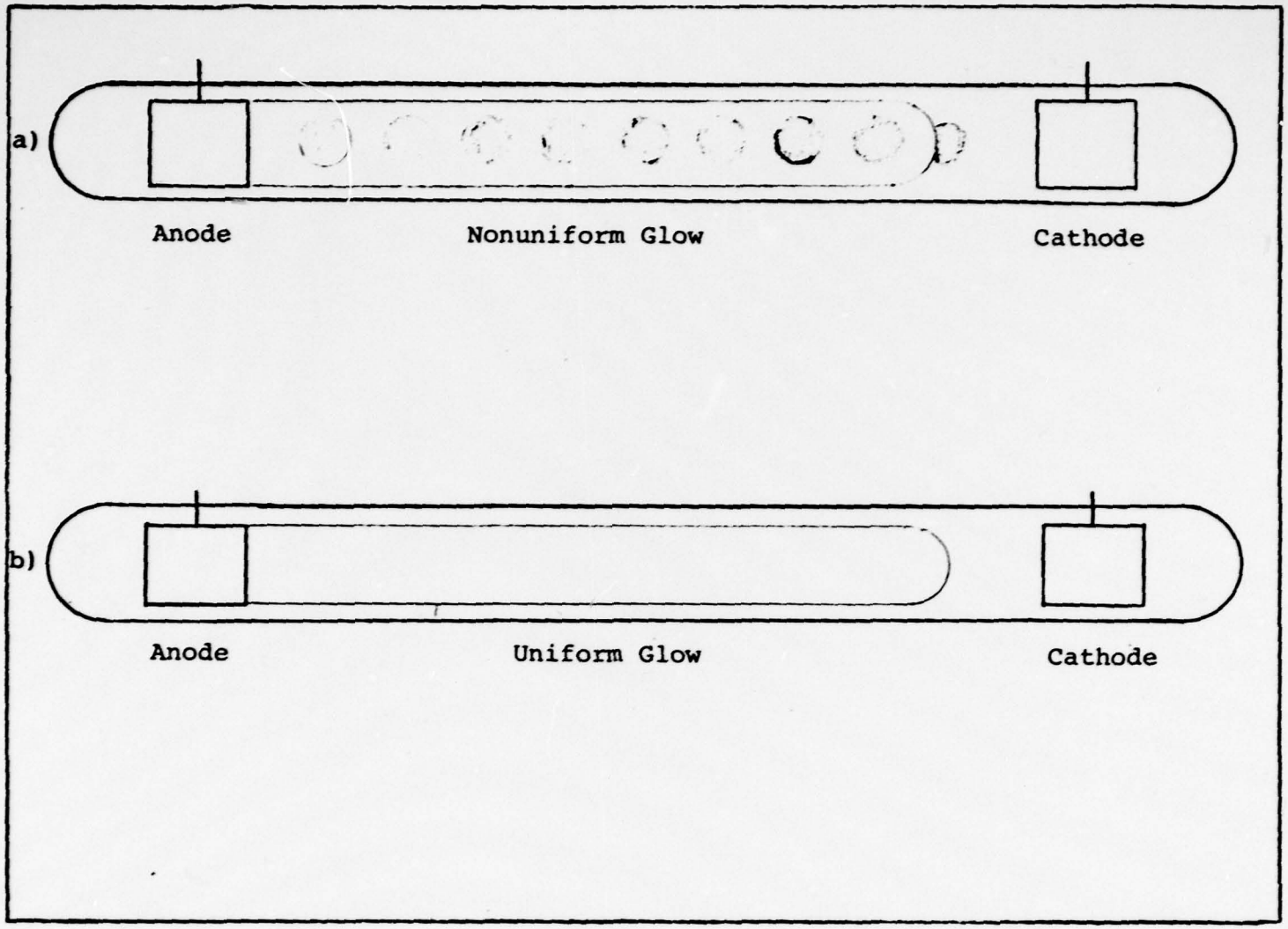

Fig. 12. Nonuniform (a) and Uniform (b) Glow

made. The camera is set to manual control and the Wavetek Function Generator activated for a triangle pulse output. The amplitude of the triangle pulse is adjusted to drive the photomultiplier across the positive column length while the oscilloscope is set so that there appears a horizontal line which moves the vertical length of the scope screen in phase with photomultiplier motion. The frequency control on the Wavetek is used to set the speed of the photomultiplier sweep and hence exposure time.

The oscilloscope is set to 1 or .5 mS time base and the screen gradicle brightened. After the desired striation frequency is set, transistor voltage is recorded and a photograph taken of the oscilloscope trace. This is done by opening the shutter while the photomultiplier sweeps from electrode to electrode. The process is repeated across various frequencies. In addition, data will be taken for other currents.

SF_6 is now introduced in trace amounts. The effect on the discharge is a change in color from light purple to orange and a constriction of the positive column. The dispersion parameters are again measured as before for various amounts of SF_6.

After the dispersion data is collected, the length of the photomultiplier sweep is measured by a ruler and the number of divisions on the gradicle swept by the oscilloscope trace counted. Dividing the sweep length by

divisions gives a conversion in cm per division for use in determining the wavelength and phase velocity from the photographs.

Photograph Analysis

To find wavelength, the length between two successive vertical intercepts is measured. The intercepts are located on the same vertical axis as shown in Fig. 13. The phase velocity involves simply finding the slope of trace.

Pulser Activation

The pulser network is turned on after a glow discharge has been established and set to desired parameters. The Thyratron is turned on and allowed to warm up. The voltage control is set to zero volts during this time. The Wavetek Function Generator is set for a square pulse signal at three Hz.

After warm up, the Thyratron voltage is slowly increased to nine kV. The loop is visually inspected to insure proper operation. The area within the voltage loop should flare with every pulse. In addition, a popping noise should also accompany each pulse.

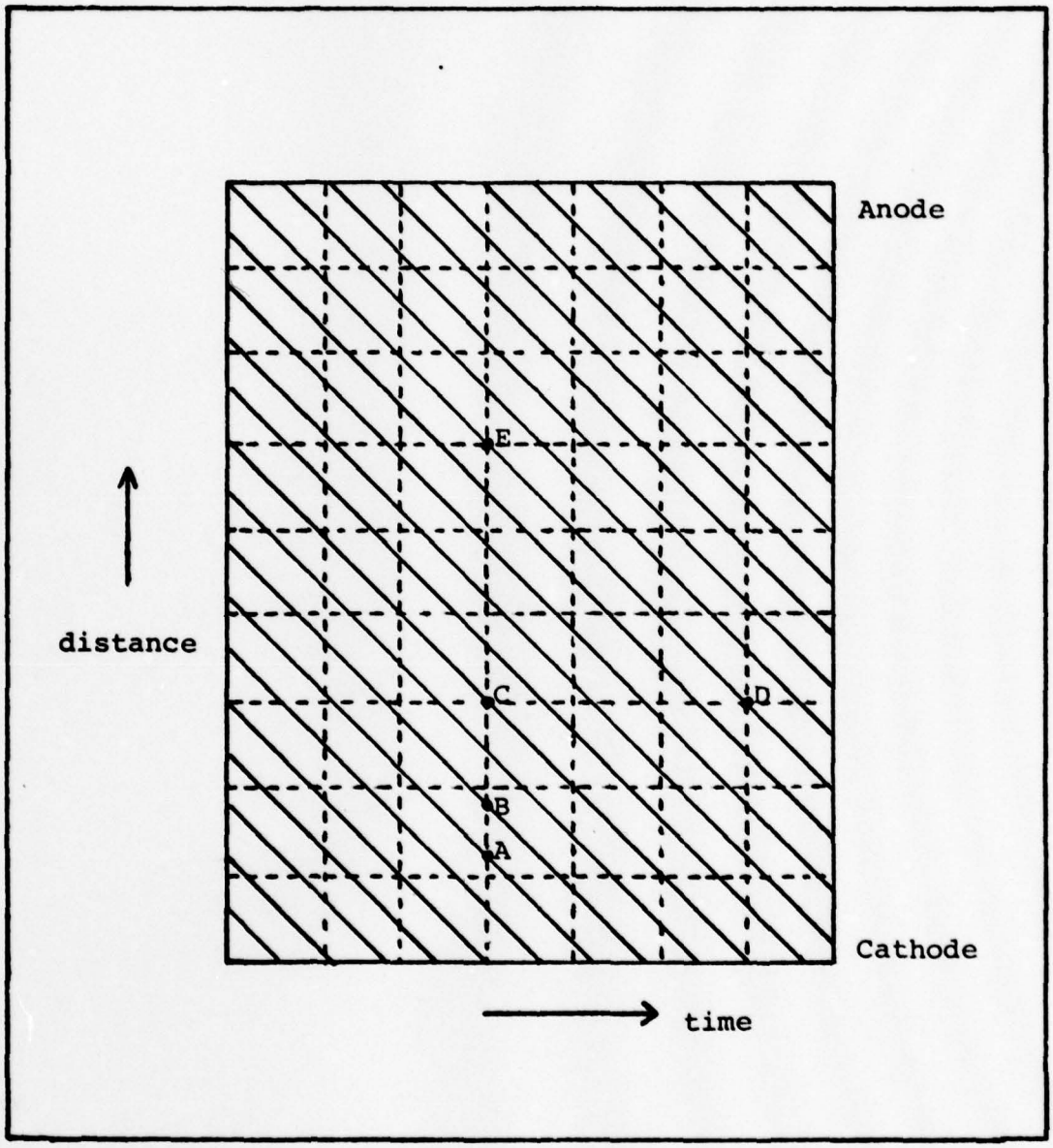

Fig. 13. Photograph Analysis

For phase velocity, distance EC is divided by the time CD. Wavelength is simply the length AB.

Pulser Data Collection

Although the same equipment for measuring is used, operations and photograph interpretation are different. Since an external trigger is used, a check is first made to see if the oscilloscope is synchronized with the pulser. This is done by applying the photomultiplier signal directly to the oscilloscope. As the photomultiplier sweeps across the tube there should be a large peak encountered near the voltage loop. The voltage of the peak should correspond with the setting on the Thyratron. Varying the trigger amplitude on the oscilloscope is tried until the correspondence is achieved.

The Thyratron voltage is set back to zero and the photomultiplier signal checked again. If there are naturally occurring wave packets in the discharge, the discharge current and oscilloscope time base are varied until either no wave packets appear, or a display showing individual striation waves completely filling the oscilloscope screen can be achieved. This is done because the wave packet caused by the pulser would be indistinguishable from the natural wave packets resulting in a jumbled and unusable photograph.

After the above procedures are accomplished, the photomultiplier signal is returned to the trace modulation input of the oscilloscope and a photograph is taken

as described earlier. The result, however, is very different as shown in Figure. 14.

Pulser Photograph Analysis

Group velocity, phase velocity, frequency, propagation direction, and wave length can be measured directly from pulser photographs.

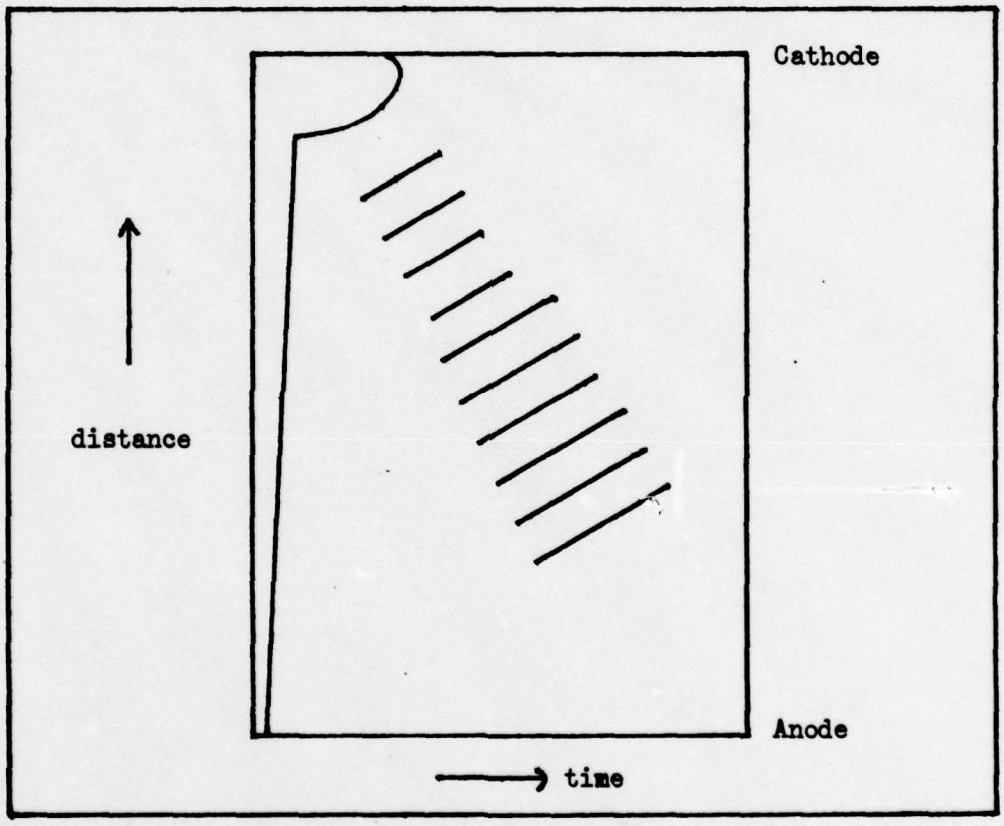

Fig. 14. Pulser Photograph Representation

The group velocity is the slope of the line bisecting the diagonal dashes while phase velocity is the slope of the dashes themselves. A more detailed look at a photographic record is shown in Fig. 15.

The frequency is the number of waves intercepting a given time axis. For example, with four waves intercepting a time axis, and with an oscilloscope time base of .5 ms/box, the frequency is 4/0.5 ms or 8 kHz. As shown in Fig. 12, the frequency varies with distance. The direction of propagation is shown to be from cathode to anode for group velocity and anode to cathode for phase velocity.

The dispersion characteristics of the waves are also shown by the photograph. Measurements of the slope giving phase velocity will vary with distance as was mentioned earlier with frequency. This will allow a plot of phase velocity and frequency to be drawn which is a measure of dispersion.

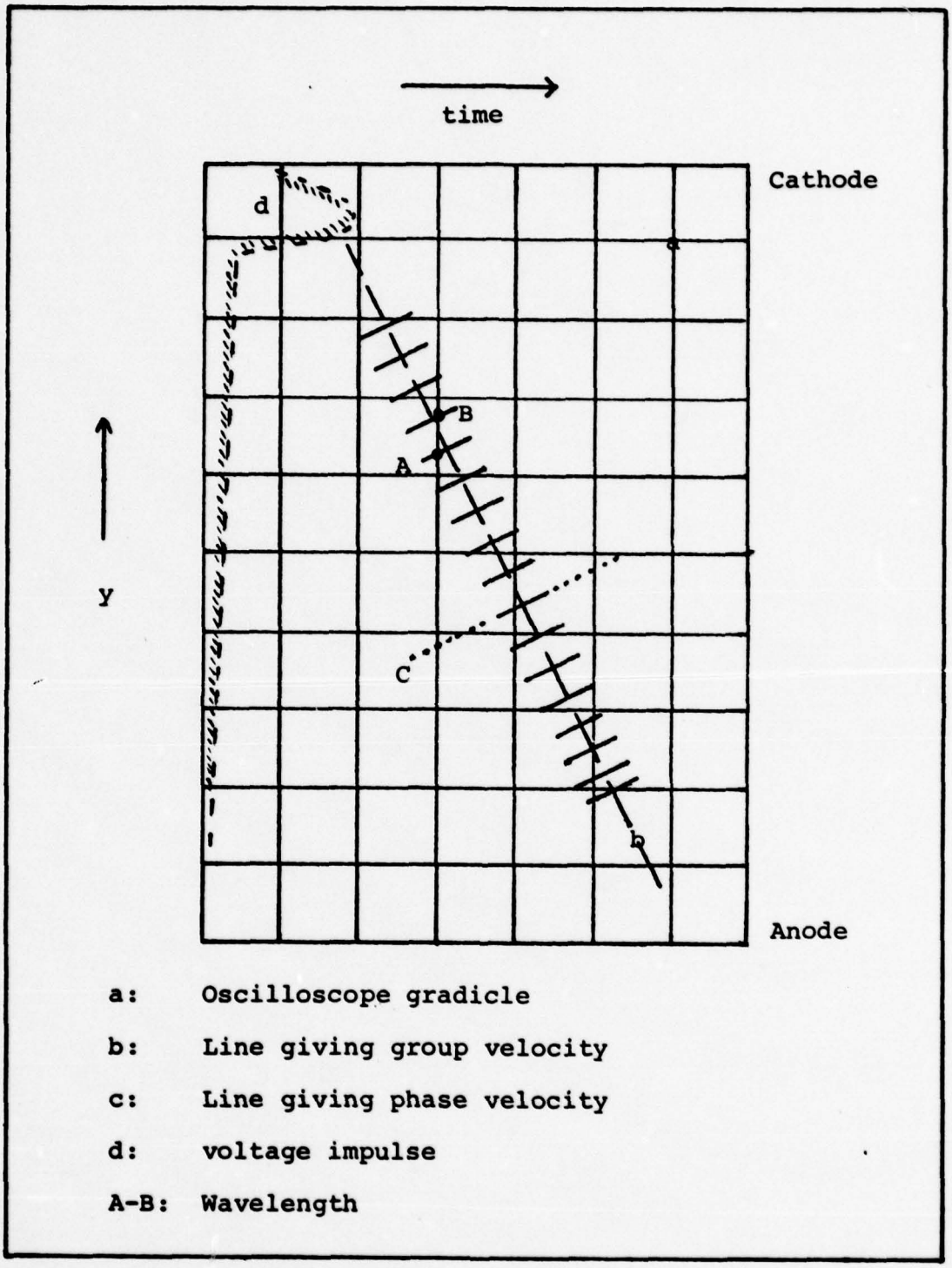

a: Oscilloscope gradicle

b: Line giving group velocity

c: Line giving phase velocity

d: voltage impulse

A-B: Wavelength

Fig. 15 Pulser Photograph Analysis

VI. Results

Introduction

Both the AC driver network and pulser network were used to obtain data on wave dispersion through various mixtures of Argon, SF_6 and CO gas. The results showed that the addition of SF_6 gas to an Argon discharge will radically affect the discharge operating voltage as well as the dispersion characteristics of the waves in the discharge. The further addition of CO gas to the Ar/SF_6 mixture indicates that the affect of the SF_6 gas on the dispersion behavior of the striations can be reduced. However, the CO addition required that the discharge operating voltage again be increased but at a lower rate for a given amount of gas than for the SF_6.

AC Driver Results. Data was taken for Argon and Argon/SF_6 discharges operated at 2 and 2.5 Torr. Discharge current was set to 8, 12, and 16 mA for each pressure while the SF_6 concentration was regulated for 0.112 and 0.224 SCCM flows compared to a constant flow of 236 SCCM for Argon. Fig. 16 and Fig. 17 show a sequence of photographic data in which pressure and SF_6 concentration are varied. In addition, the electrode functions have been reversed for Fig. 17. All the photographs show that the phase velocity proceeds from the anode to the

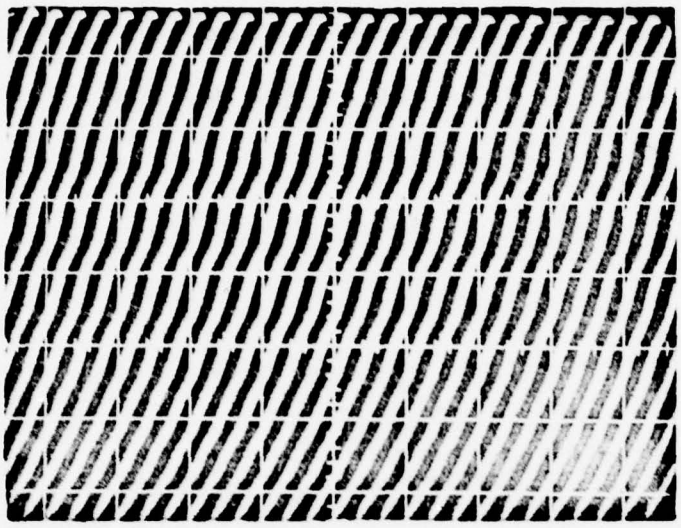

Cathode

0.5 mS/division

Anode

I = 12mA P = 2.5 Torr
0.112 SCCM SF_6 236 SCCM Argon

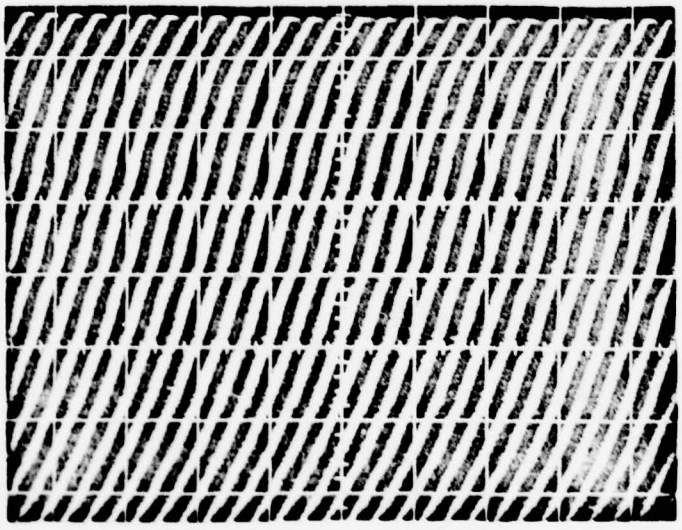

Cathode

0.5 mS/division

Anode

I = 12mA P = 2 Torr
0.122 SCCM SF_6 236 SCCM Argon

Fig. 16. Argon/SF_6 AC Driver Data

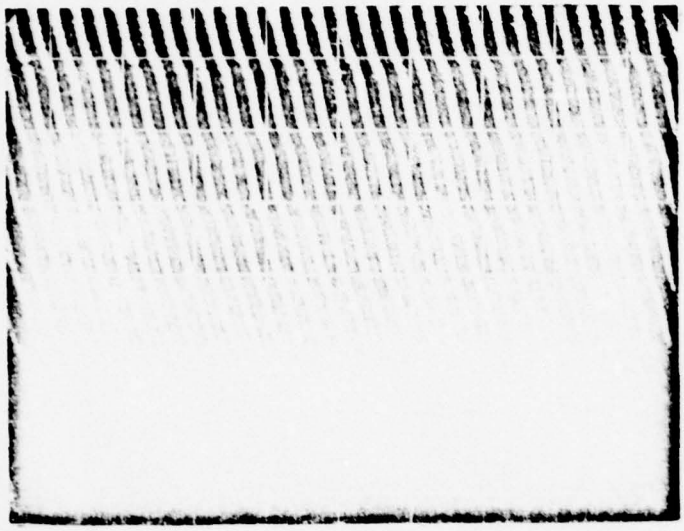

Anode

0.5 mS/division

Cathode

I = 12mA P = 2.5 Torr
0.224 SCCM SF_6 236 SCCM Argon

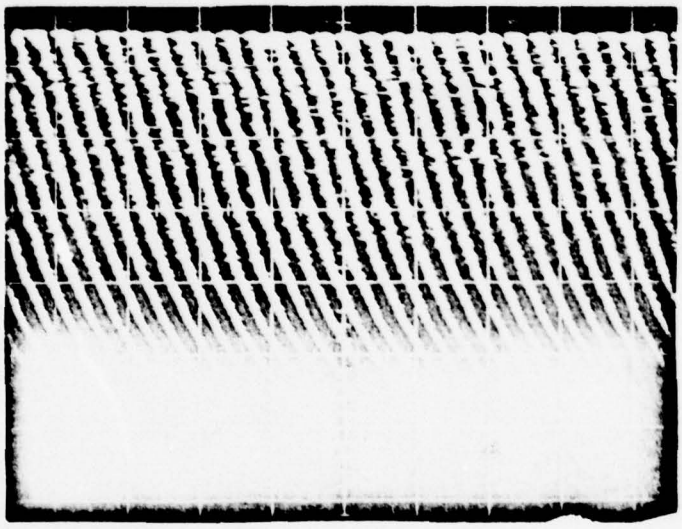

Anode

0.5 mS/division

Cathode

I = 12mA P = 2 Torr
0.224 SCCM SF_6 236 SCCM Argon

Fig. 17. SF_6 Damping Effect

cathode. Comparisons between the photographs show that as the SF_6 concentration is increased, the wave disturbances near the cathode end are no longer visible. With the pulser network, it will be shown whether the waves attenuate toward the cathode or have not had sufficient gain in traveling toward the anode.

The modulations visible in the waves are due to Van der Pohl oscillations as the frequency sweeps across the maximum gain point. The change of slope evident toward the top and bottom of the photographs is due to local anisotropies in gas mixing.

As SF_6 was introduced into the Argon discharge, the operating voltage increased markedly. Fig. 18 illustrates the voltage increase caused by the addition of just a trace of SF_6.

Analysis of the photographs showed only slight changes in wave number with changes in driving frequency. As the SF_6 concentration was increased, the relation between phase velocity and driving frequency greatly changed. The slope of the linear plot relating phase velocity to frequency decreased indicating lower dispersion as a given difference in frequency resulted in a reduced change in phase velocity. An attempt to observe a reversal of phase velocity direction was not successful. As the concentration of SF_6 was further increased, the striations decreased in amplitude and became incoherent in both space and time. This was noted by observing the

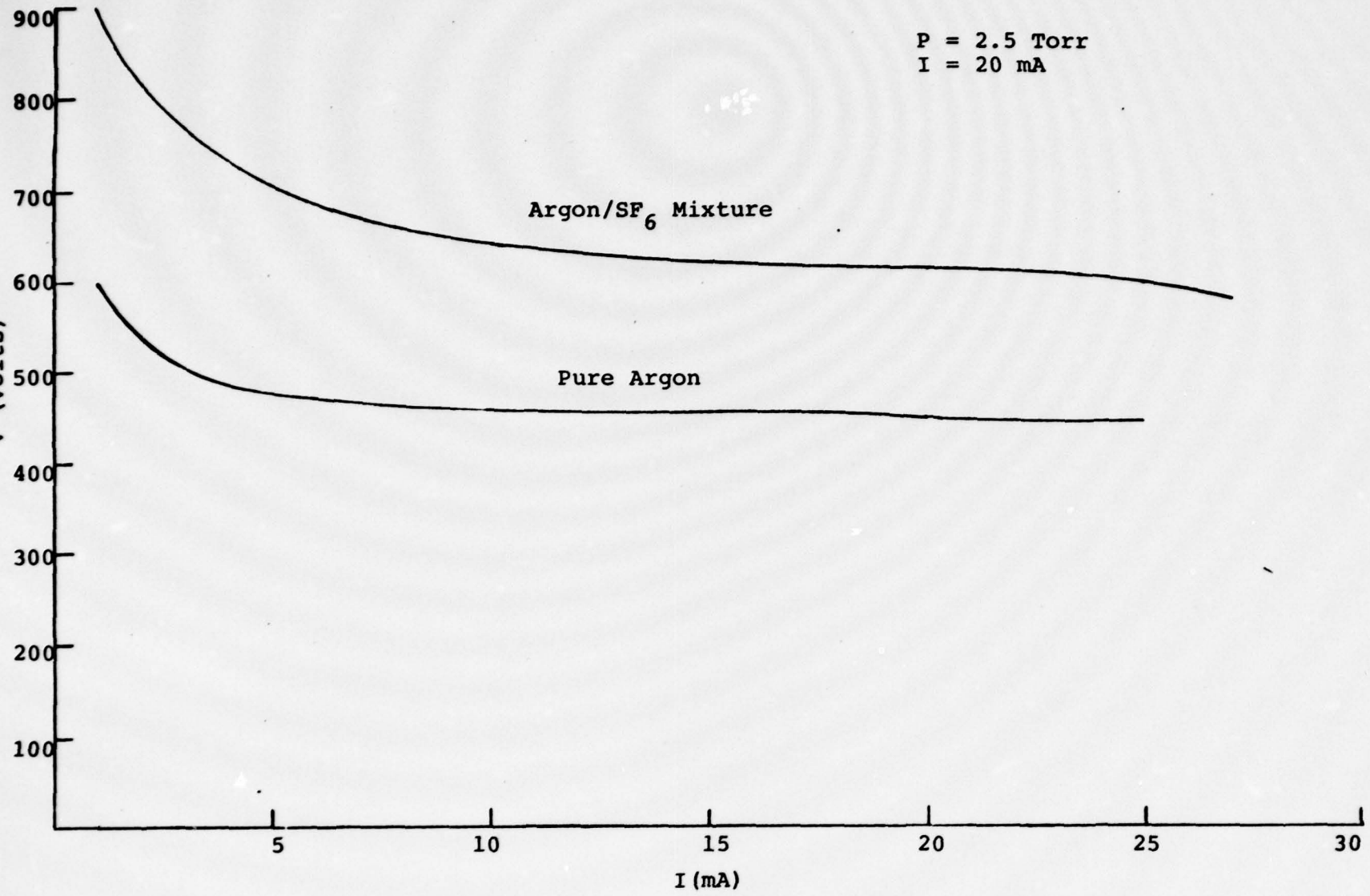

Fig. 18. Current-Voltage Effect

direct photomultiplier signal on the oscilloscope. The wave trace representing the striation changed from a sinusoidal pattern to a jumbled mixture of many traces each triggering at different points. The amplitude of each trace descreased with increasing concentrations of SF_6 and eventually the traces resembled noise signals.

Fig. 19 shows a sequence of photographs representing the affects of SF_6 on the Argon discharge just below the concentration at which the striation trace degraded beyond the recordable stage (the point at which the signals were no longer coherent and too weak for brightness modulation). An addition of one SCCM of CO was added to the above mixture and the results are shown in Fig. 20. The graph shows phase velocity plotted against the striation frequency. The Ar/SF_6 approached but did not cross over the frequency axis. As a result, the vertical intercept occurs at a negative velocity indicating backward waves. Attempts to obtain data showing such a cross over to forward wave types were not successful for the above discussed problem.

Additional data on pure Argon and Ar/SF_6 mixtures are shown in Figs. 21 to 22. The graphs illustrate the decreased didpersion obtained when SF_6 is added to the Argon discharge.

The negative intercept on the dispersion plots indicate backward waves: group and phase velocity in

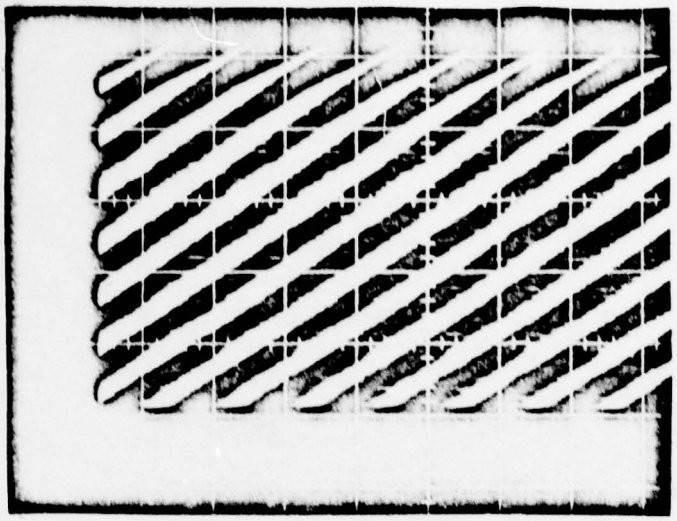

I = 25mA P = 2.5 Torr 236 SCCM Argon
900 Volts f = 9kHz

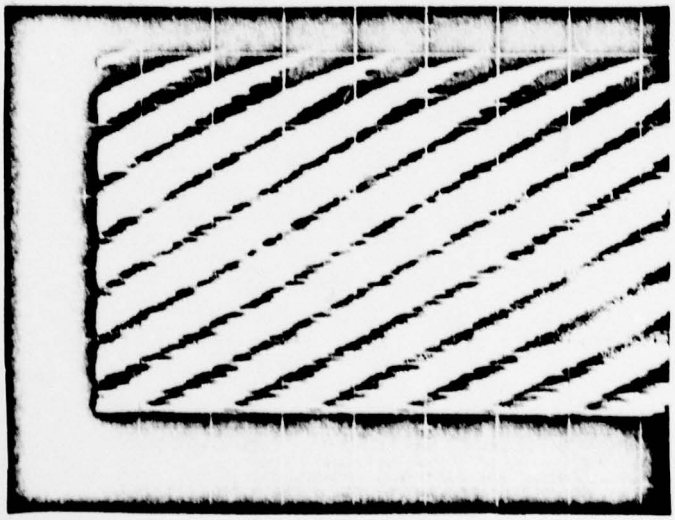

I = 25mA P = 2.5 Torr 236 SCCM Argon
900 Volts f = 8 kHz

Fig. 19. Maximum Usable SF_6 Concentrations

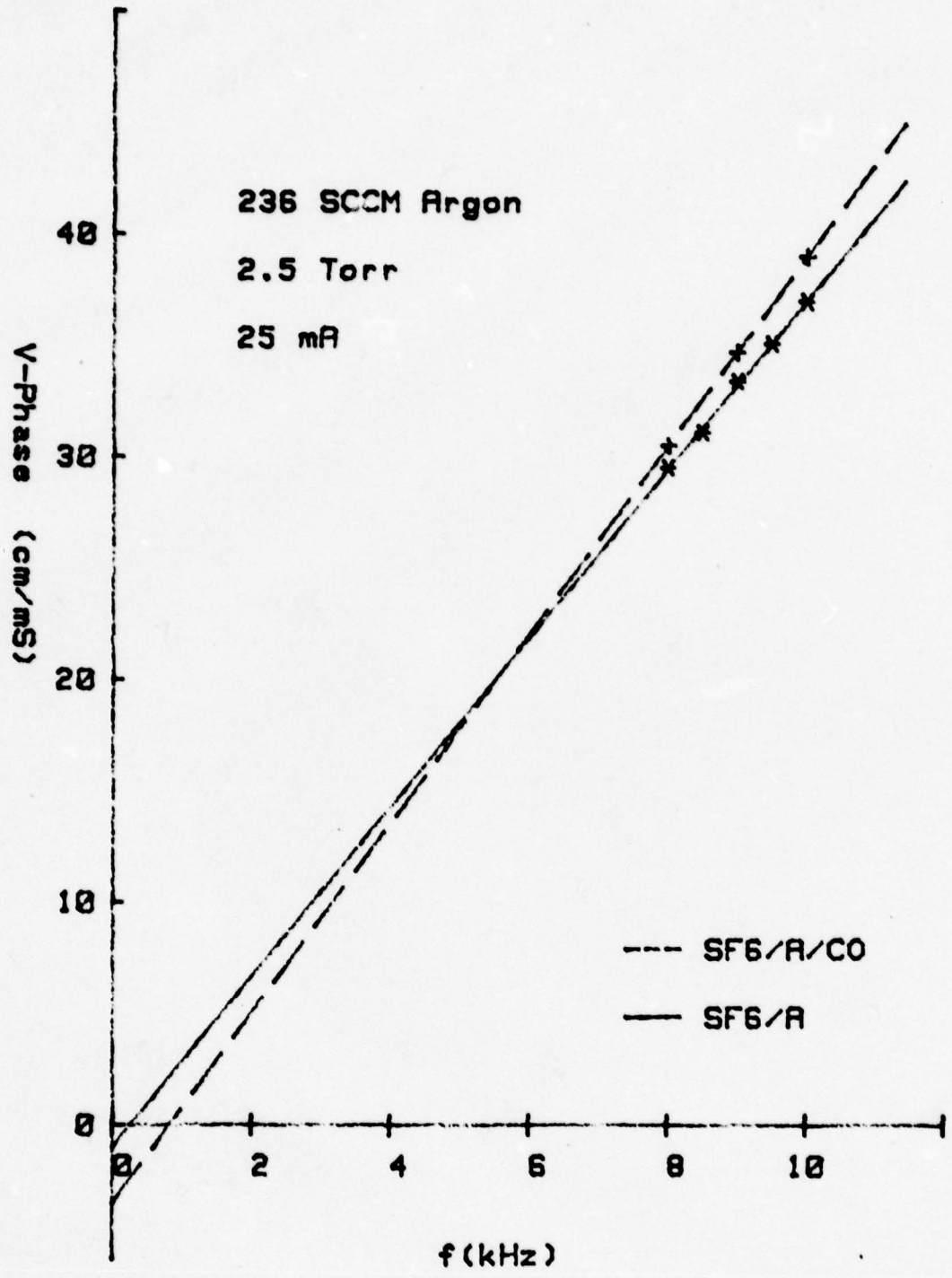

Fig. 20 . Current Modulation Results

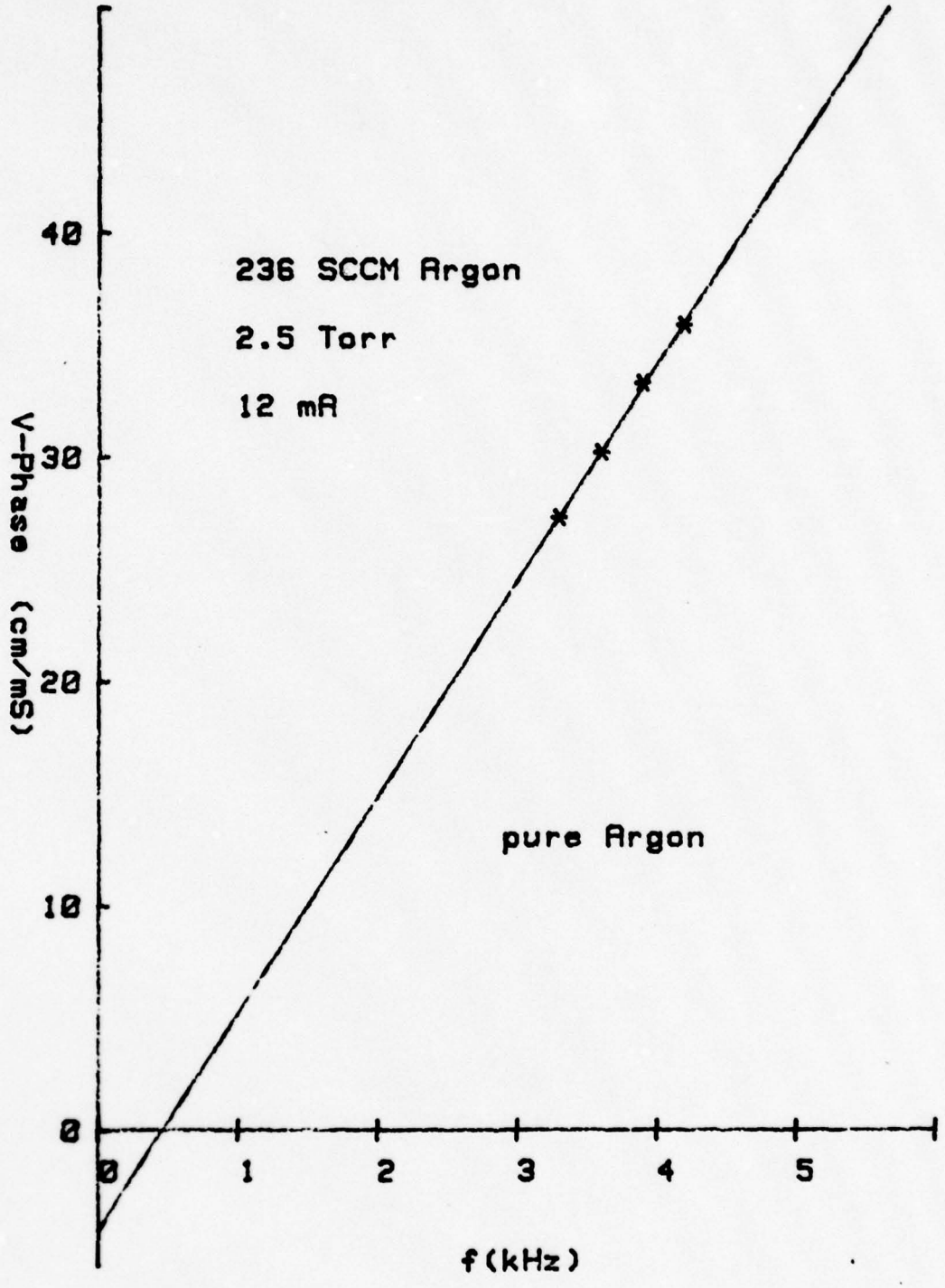

Fig. 21. Argon Dispersion

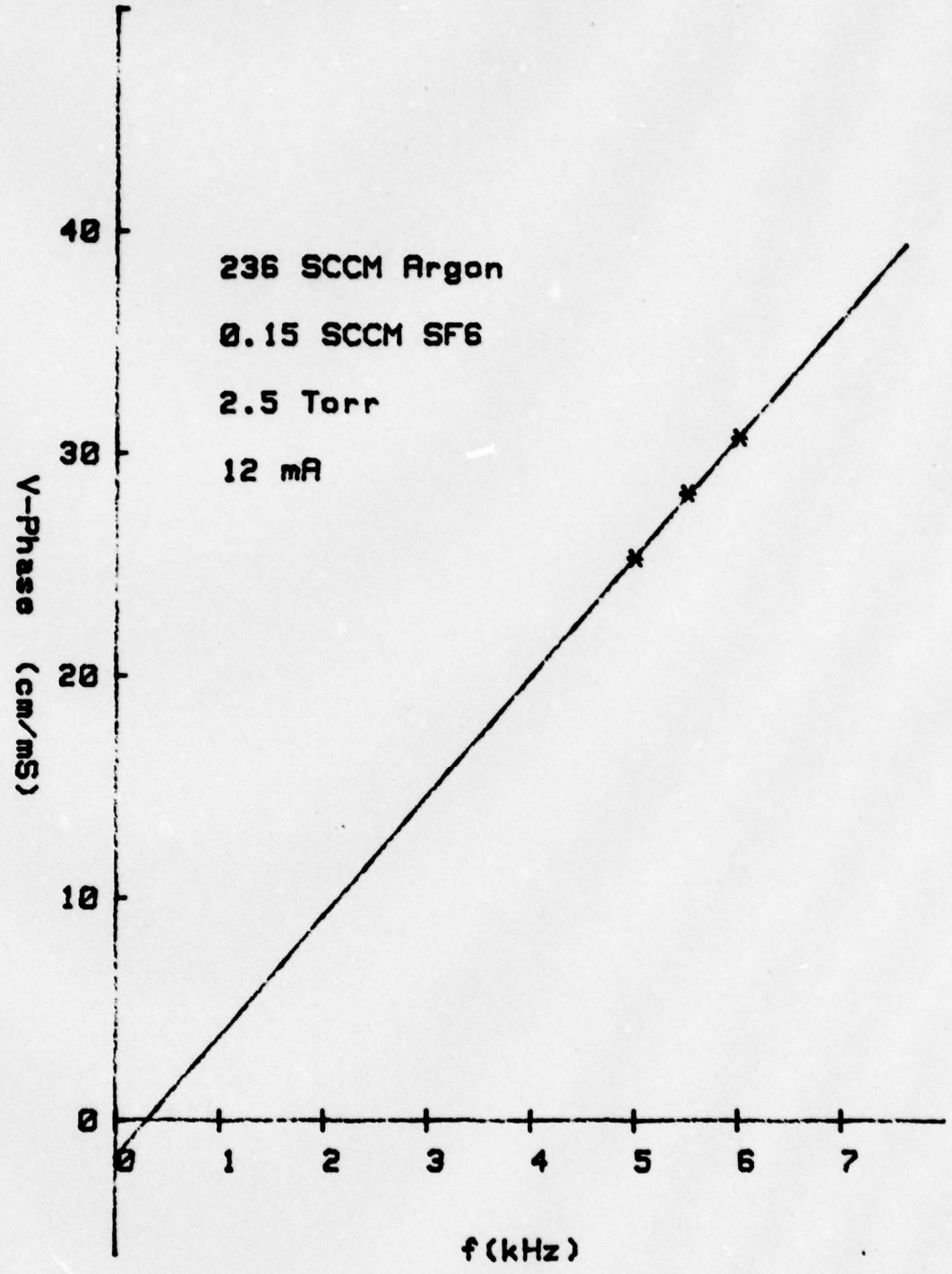

Fig. 22. Argon/SF_6 Dispersion

opposite directions. The magnitude of the intercept is approximately the value of the group velocity (see Appendix B).

Pulser Results. The pulser was operated with the same discharge parameters used before. The pulser itself was operated between 8 to 10 kV per pulse at a frequency of 2 or 3 Hz. Several typical pulser photographs are shown in Fig. 23. The photographs differ in that phase velocity lines appear sometimes within, outside or both inside and outside of the pulser induced wave packet. The difference depends upon the parameters of naturally occurring wave packets. If these parameters are too close to the pulser wave packet, the discharge current is adjusted until the pulser wave packet can be distinguished against the discharge background.

The gas mixtures tested with the AC voltage drives were retested with the pulser. The results showed that the group velocity travels from cathode to anode opposite to the phase velocity. Figs. 24 and 25 show a sequence of photographic data. The wave packets generated by the pulser are easily distinguished. The occasional branching or duplicating of the wave packet is due to nonlinear superposition of the driven and natural wave packets and not the r and s wave branching.

All the photographs showed the backward wave nature indicated by the negative intercepts on the AC

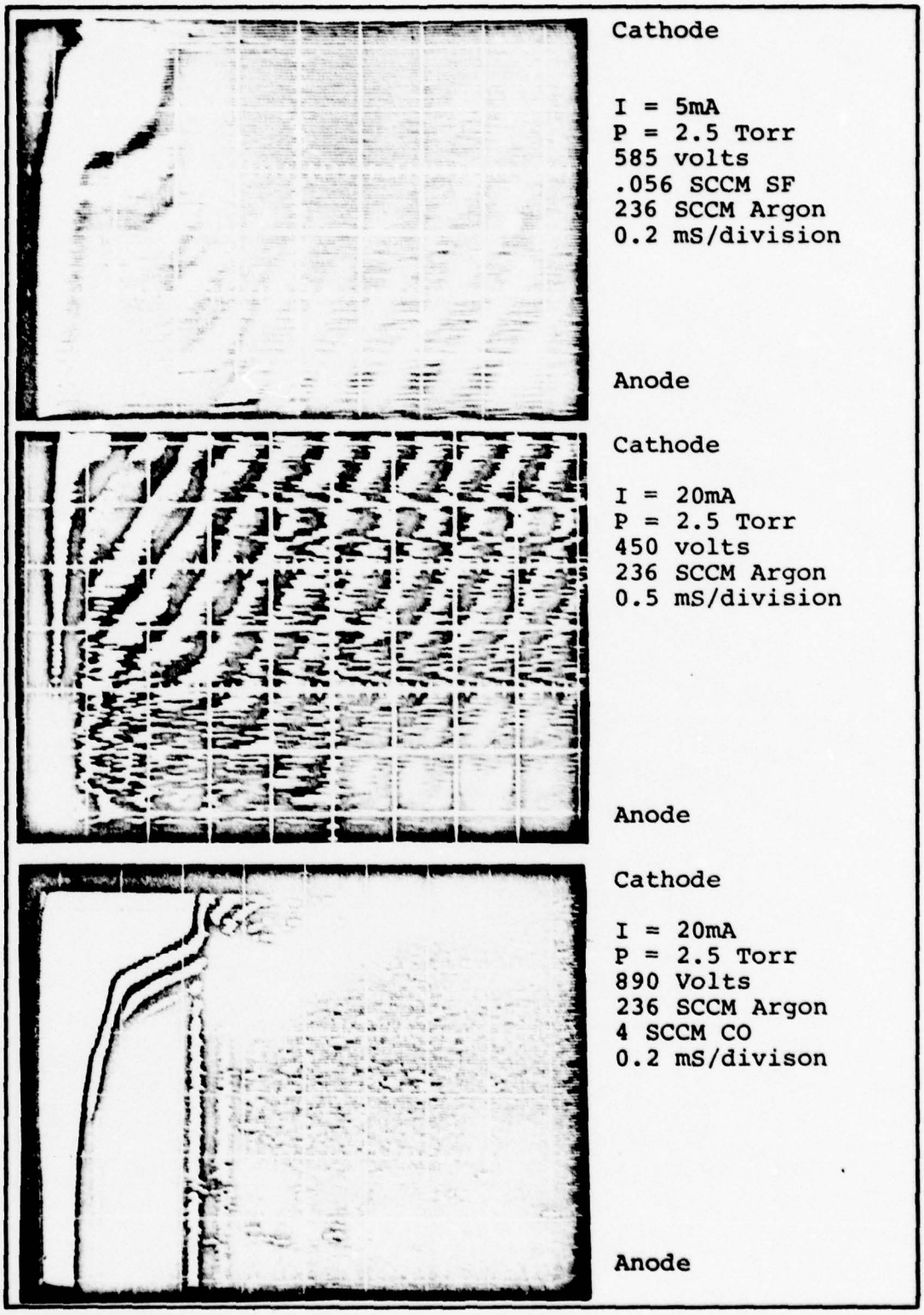

Fig. 23. Typical Pulser Photographs

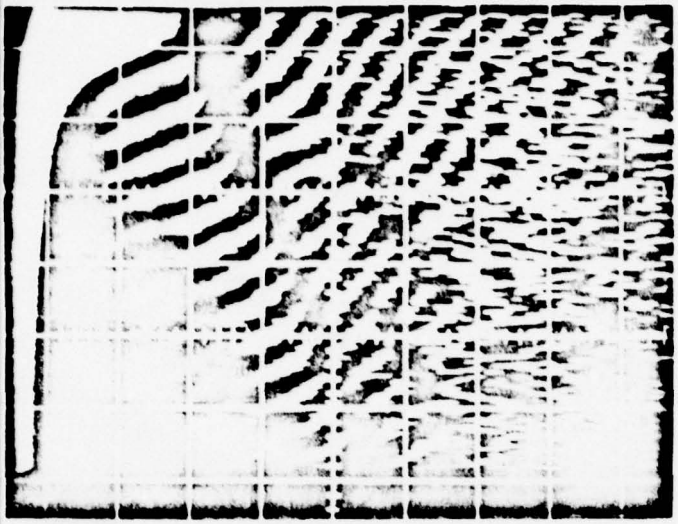

Cathode

.2mS/division

Anode

I = 11 mA P = 2.5 Torr 236 SCCM Argon
.056 SCCM SF_6 .75 SCCM CO

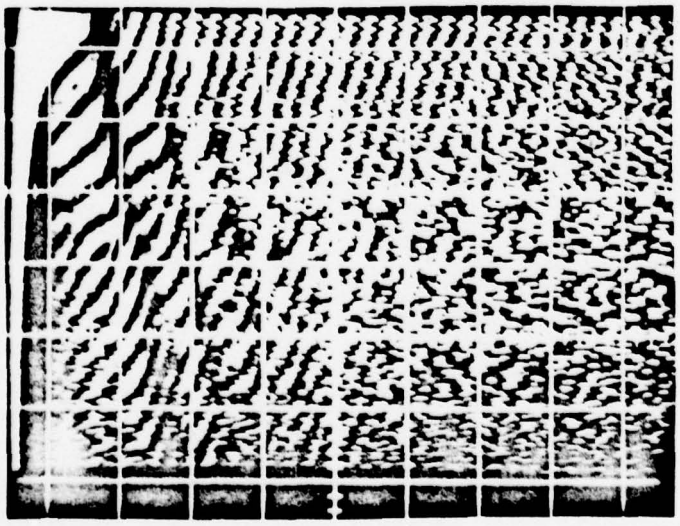

Cathode

0.5mS/division

Anode

I = 11 mA P = 2.5 Torr 236 SCCM Argon
.056 SCCM SF_6 .5 SCCM CO

Fig. 24. $Ar/SF_6/CO$ Pulser Data

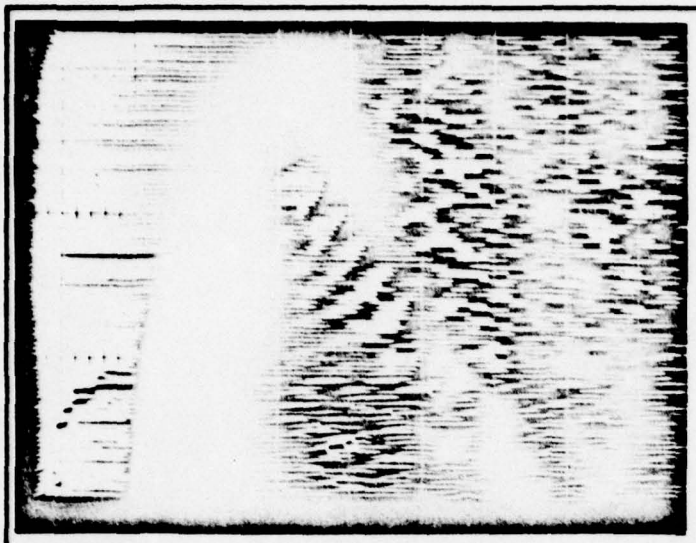

Cathode

0.2mS/division

Anode

I = 5 mA P = 2.5 Torr
236 SCCM Argon .75 SCCM CO

Cathode

.2mS/division

Anode

I = 20 mA P = 2.5 Torr
236 SCCM Argon 2 SCCM CO

Fig. 25. Ar/CO Pulser Data

driver graphs. Obtaining data on forward waves was prevented by the same reasons discussed earlier. Fig. 26 shows the result of SF_6 suppression of striations on a pulser photograph. No phase velocity lines are visible for analysis either within or outside the wave packet.

The group velocity given by the pulser photograph gives the slope for only the wave number and frequency corresponding to the maximum point of the gain curve associated with the particular gas mixture. A gain curve is shown for pure Argon in Fig. 27. The maximum gain is found at the vertex of the parabolic gain curve.

The voltage pulser produces an extremely narrow square pulse waveform. The square wave is itself a superposition of many different sinusoidal waves of differing frequencies. The frequency closest to the point of maximum gain is the one which will dominate and determine the frequency of the resulting striation. If there are several frequencies close to maximum gain frequency, then several competing nodes may result with the discharge.

The results of the pulser data are shown in Figs. 28 and 29. The graphs shown correspond with the AC Driver results in that the addition of SF_6 results in reduced dispersion. On an w versus k plot, this is represented by a steeper slope.

As the SF_6 is introduced, the slope increases. Further addition of CO to the Ar/SF_6 mixture results in

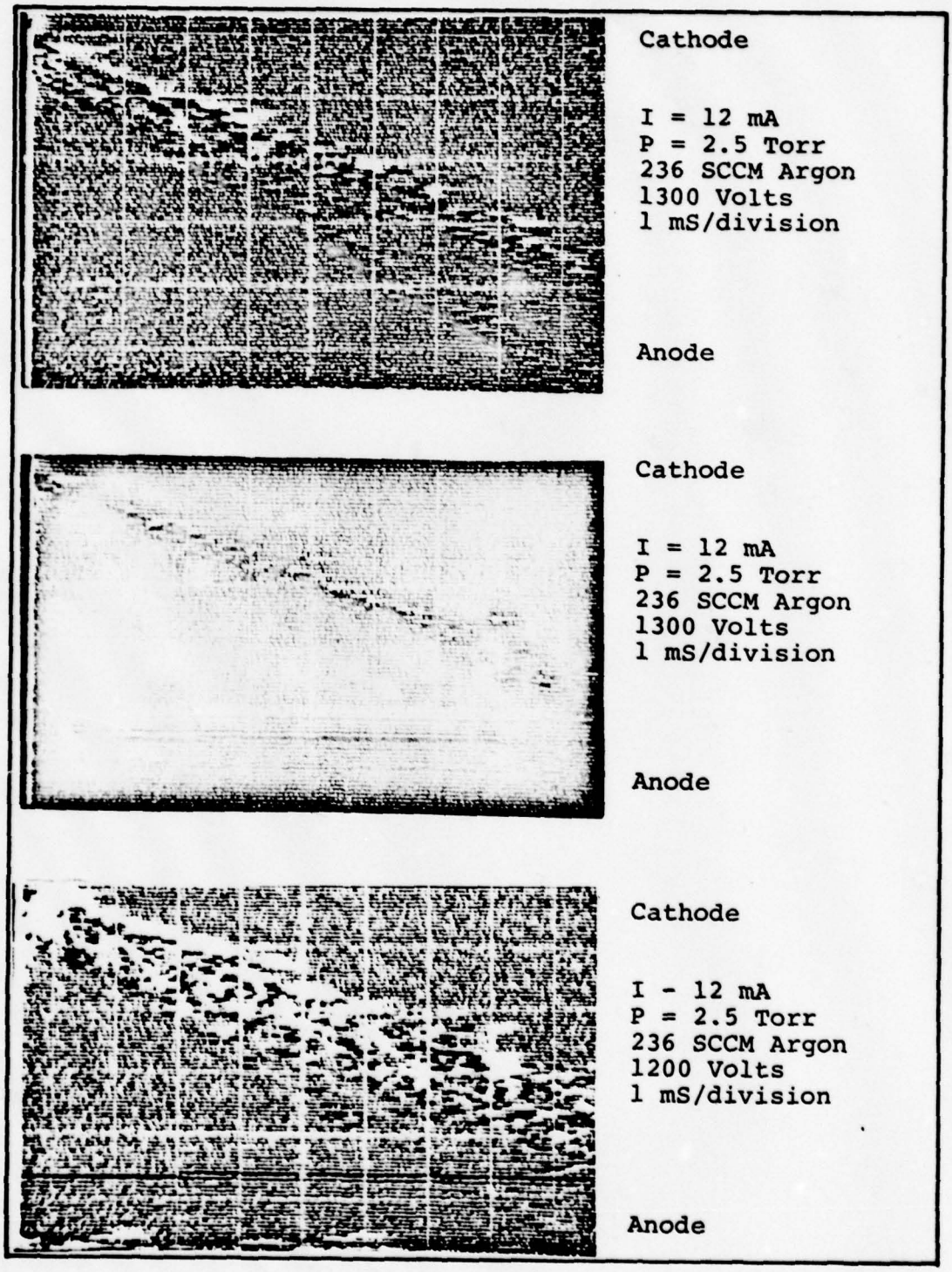

Fig. 26. SF_6 Suppression Effects

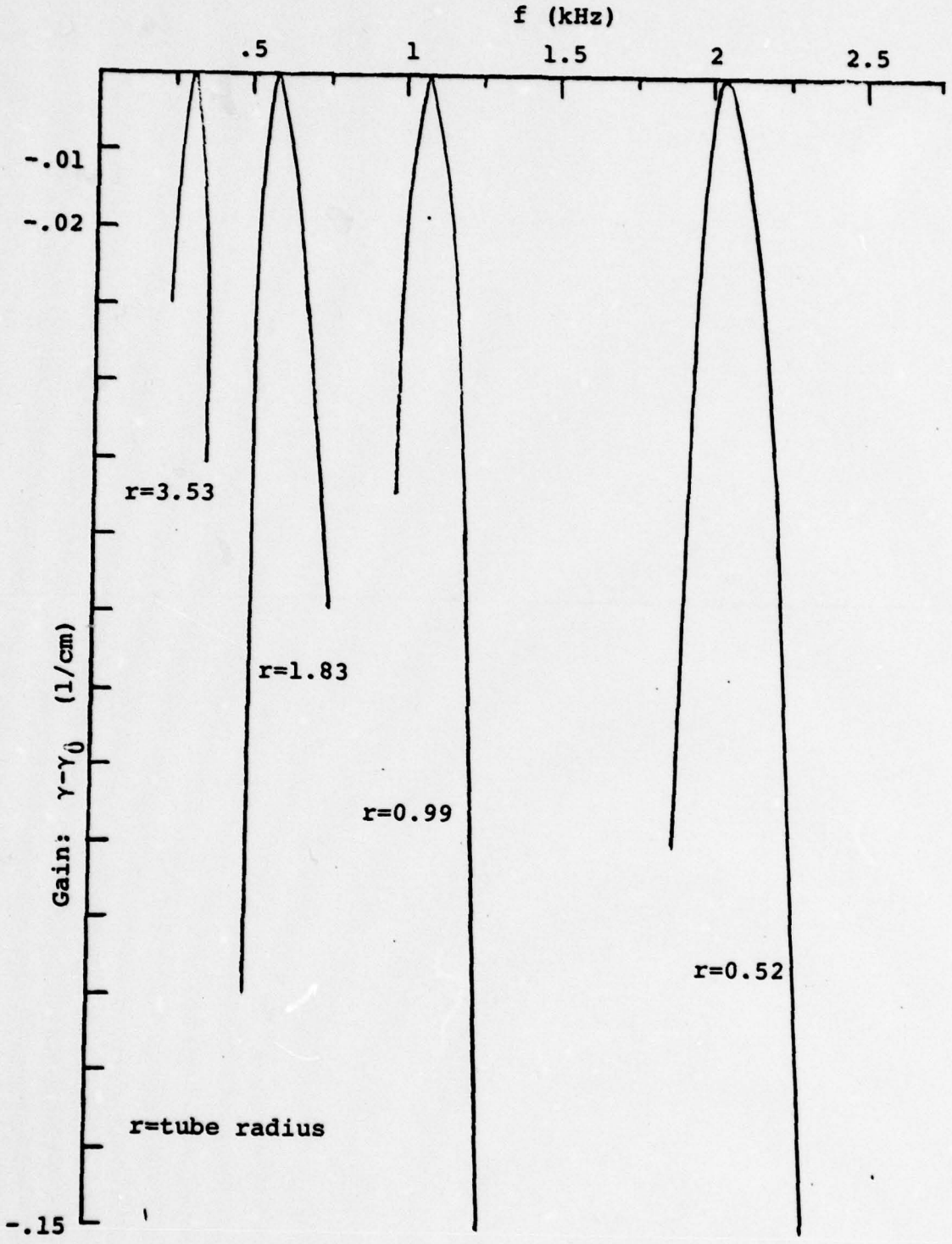

Fig. 27. Argon Gain Curve

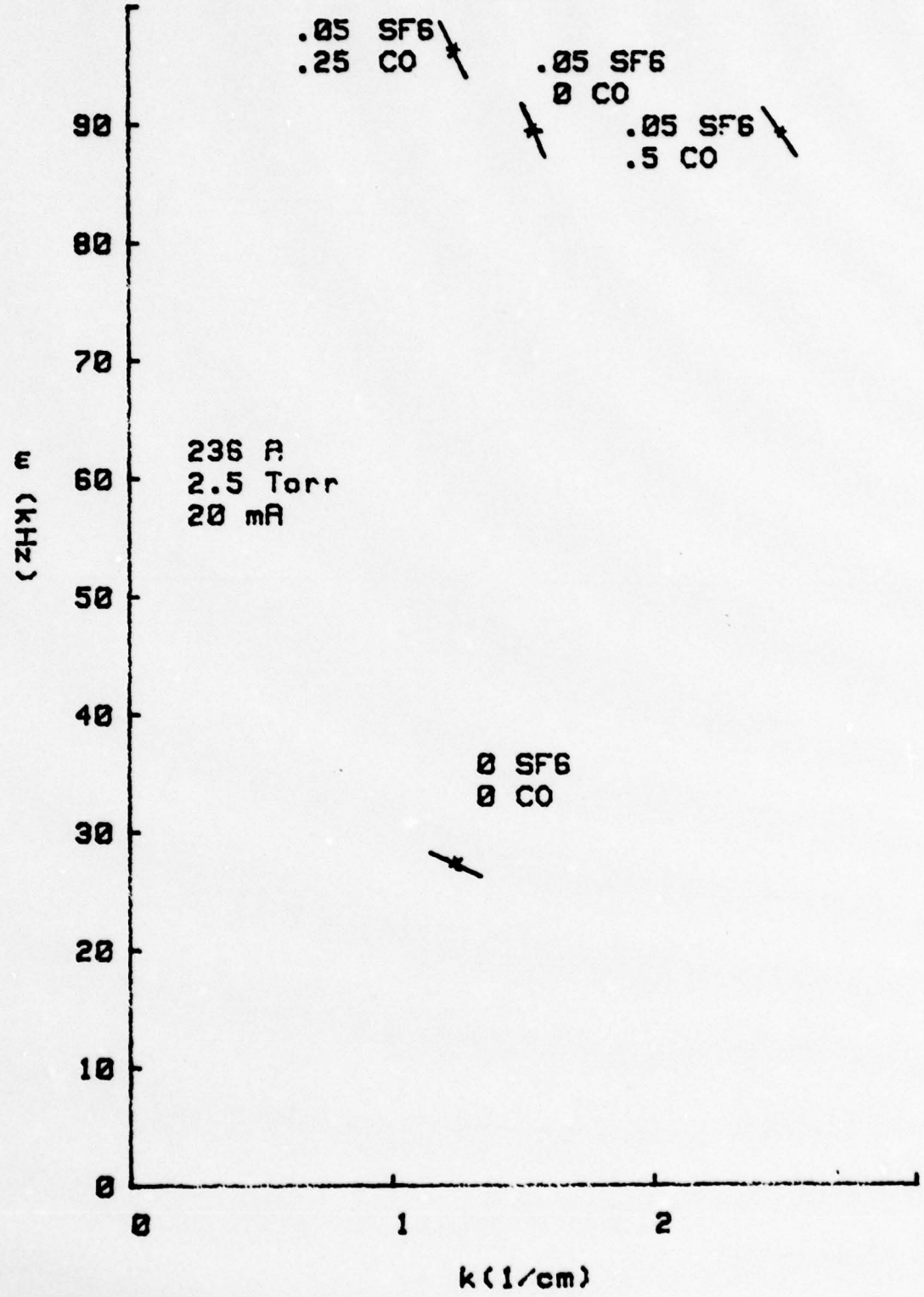

Fig. 28 . Voltage Pulser Results

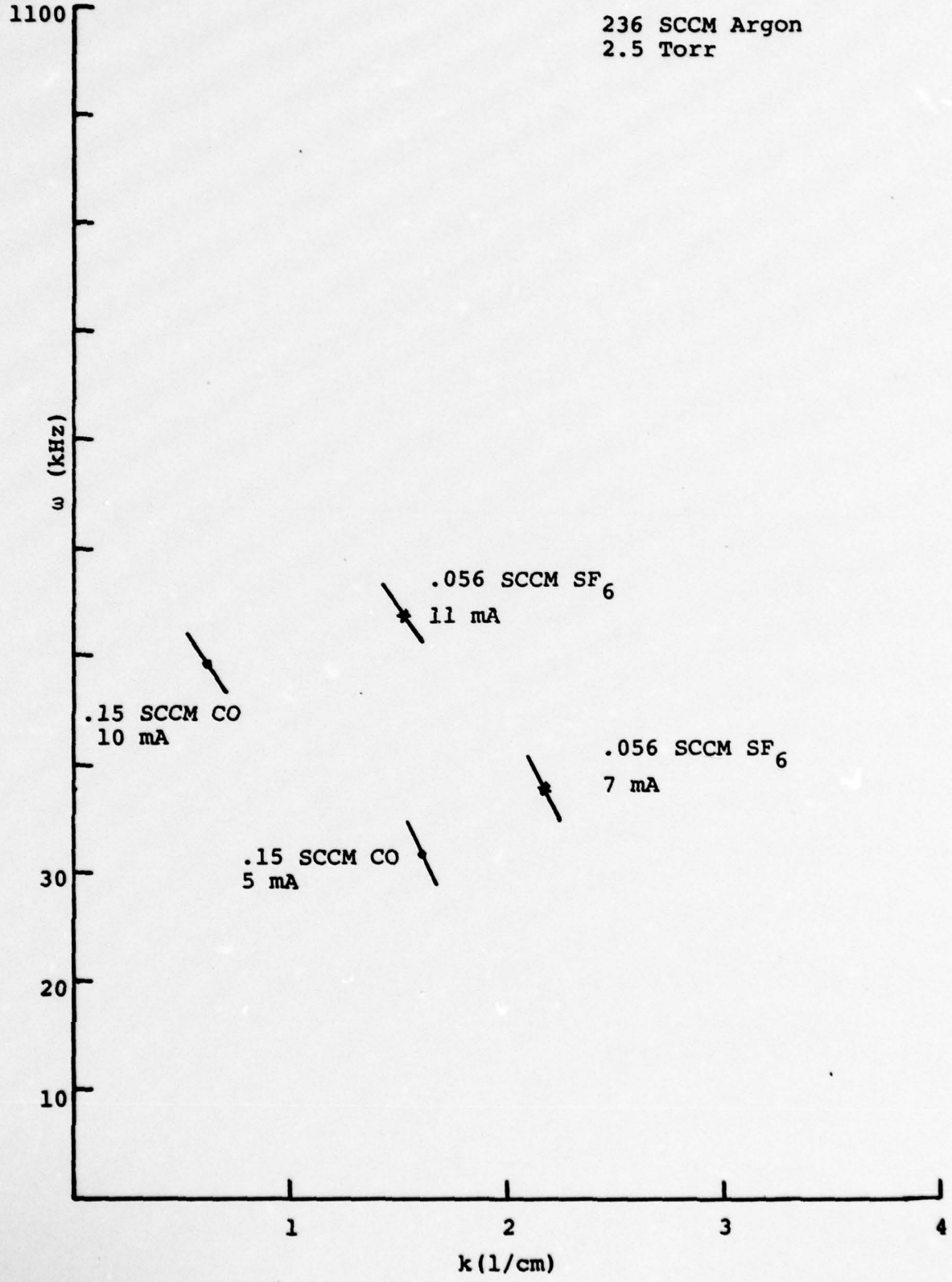

Fig. 29. Current Effects on Dispersion

the slope decreasing in angle back to the original Argon only value. However, the w,k point for the maximum gain remains shifted into higher values. The addition to CO causes this shift to increase rather than to reduce the SF_6 induced shift.

Reference tests were also made with an Ar/CO mixture to determine the effects of CO alone on an Argon discharge. The results showed that the CO gas also decreased the dispersion of the discharge. But as the CO concentration was progressively increased, the dispersion began to increase again.

Fig. 30 shows the plot of various mixtures of Argon and CO. As can be seen, the slope of the w versus k plot jumps sharply with the addition of slight traces of CO but begins to decrease as more CO is added. In addition, the maximum gain point is continuously shifted to larger w and k values as the CO is added.

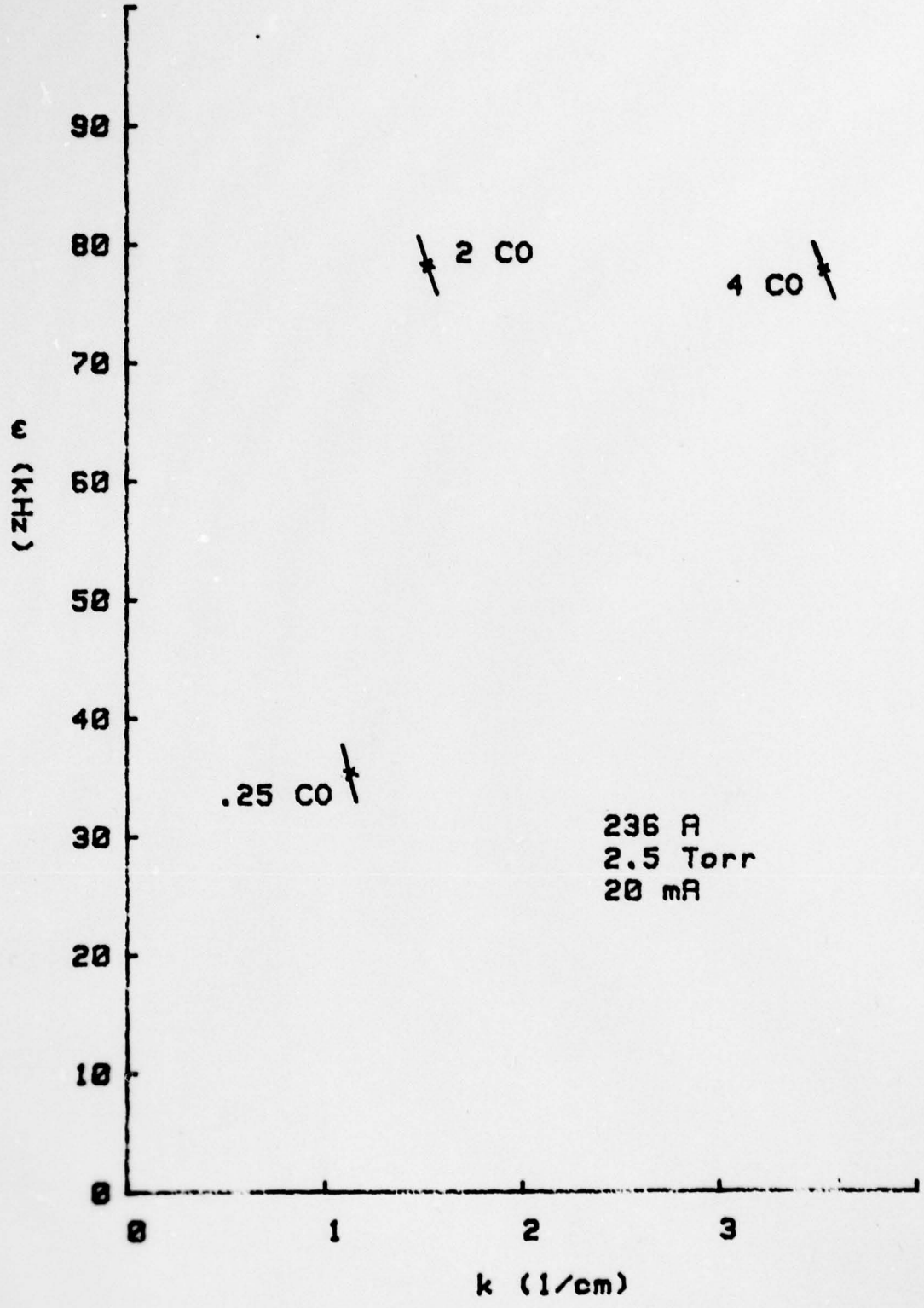

Fig. 30. Argon/CO Dispersion

VII. Conclusions and Recommendations

Summary

Using both current modulation and voltage pulsing techniques with space-time oscillograms, backward waves were measured in mixtures of Argon, sulfurhexaflouride, and carbon monoxide gas. It was seen that the introduction of negative ions into the Argon discharge reduced the dispersion of the moving striations in the positive column and was tending to reverse the direction of propagation for phase velocity as noted by graphs showing vertical intercepts approaching the frequency axis with the addition of SF_6.

It was also observed that the addition of CO to the Ar/SF_6 mixture tended to reduce the effect of SF_6 on the dispersion of striation waves. However the maximum gain point was seen to constantly increase its frequency and wave number value with the addition of either CO or SF_6.

The operating voltage for the discharge also increased with the addition of either SF_6 or CO but at different rates with the SF_6 producing a much higher voltage increase for a given amount of gas added.

As the amount of SF_6 reached levels of 2 percent and more of the gas mixture, the striations changed from a

single mode pattern to a random, incoherent pattern of no one single dominant mode. This made observation of phase velocity impossible using the brightness modulation technique.

Recommendations

Using the voltage pulsing technique, it should be possible to observe phase velocity lines within the disturbance area generated by the voltage impulses if the impulses are driven at high enough voltage and frequency. The pulser used for this research was limited to 10 kV and three Hertz. If the voltage impulses were driven at higher voltages and frequencies, a steady wave pattern capable of brightness modulating the oscilloscope might have been made. A linear amplifier with a very high, adjustable gain could also be used as a means to obtain brightness modulation where no strong wave mode exists. The use of such equipment should allow observation of a change from backward to forward waves as SF_6 is added to the Argon discharge. The addition of CO should show a return to backward wave behavior.

Conclusions

The use of negative ions in a glow discharge is useful for reducing the dispersion characteristics of ionization waves but only if introduced in trace amounts. The addition of more than just trace amounts causes the

breakdown of single mode oscillation and the generation of random striations incoherent in both time and space. An artifically generated disturbance will produce striations which can be directly opposite in nature to striation waves without the presence of negative ions. That is, the waves can be forward rather than backwards if the negative ion concentration is high enough.

Bibliography

1. Alanakyan, Yu. R. "Kinetic Theory of Ionization Waves." Soviet Physics Technical Physics, 22:328-330 (March 1977).

2. _____, and B. V. Vainer. "Ionization Oscillations in a Plasma with Negative Ions." Soviet Physics Technical Pysics, 18:441-447 (October 1973).

3. Asundi, R. K., and J. D. Craggs. PHYPRO 33 V83:611 (1964).

4. Dzhuvarly, Ch. M., G. V. Vechkhaizer, Yu. V. Gorin, and P. N. Mokhtizade. "Mobility of Positive and Negative Ions in Electronegative Gases." Soviet Physics Technical Physics, 22:314-315 (March 1977).

5. von Engle, A. Ionized Gases (second edition). Oxford: Clarendon Press, 1965.

6. Francis, G. "The Glow Discharge at Low Pressure." Handbook of Physics, Vol. 22:53. Berlin: Springer-Verlag (1956).

7. Garscadden, A., and P. Bletzinger. "Feedback Experiments on Multimode Ionization Waves." AIP Conference Proceedings Feedback and Dynamic Control of Plasmas: 149-159 (1970).

8. Garscadden, A. "Ionization Waves in a Glow Discharge." Gaseous Electronics, 1:65-107 (1978).

9. Haas, R. A. "Plasma Stability of Electric Discharges in Molecular Gases." Physical Review A, 8:1017. 1043 (August 1973).

10. Jones, U. F. The Glow Discharge. London: Methuen & Co., Lts., 1966.

11. Krasa, J., and L. Pekarek. "Measurement of Complicated Cures of Ionization Waves (Striations)." Czechoslovakian Journal of Physics, 23:863 (1973).

12. Krejci, V., and L. Pekarek. "Determination of Dispersion Curve Parameters from Transient Waves." Czechoslovakian Journal of Physics, 17:443-452 (1967).

13. Lee, D. A., and A. Gascadden. "Forward and Backward Wave Moving Striations in a Constricted Discharge." International Journal of Electronics, 20:256-581 (1966).

14. Long, W. H., Jr. "Discharge Stability in e-Beam Sustained Rare-Gas Halide Lasers." Journal of Applied Physics, 50:168-172 (January 1979).

15. Massey, H. S. W. Negative Ions (second edition). Cambridge: University Press, 1950.

16. Milloy, H. B., R. W. Crompton, J. A. Rees, and A. G. Robertson. "The Momentum Transfer Cross Section for Electrons in Argon in the Energy Range 0-4 eV," Australian Journal of Physics, 30:61-72 (February 1977).

17. Nighan, W. L., and W. J. Wiegand. "The Influence of Negative Ion Processes on the Stability of Molecular Gas Discharges." UAR-N23, Feburary 1974.

18. Pavlov, P. A., and V. E. Privalov. "Striations in a Glow Discharge." Soviet Physics Technical Physics, 23:775-778 (July 1978).

19. Pekarek, L., K. Masek, K. Rohlena. "A Theory of Ion-Guided and Metostable-Guided Varieties of Ionized Waves (Striations)." Czechoslovakian Journal of Physics, 20:879-894 (1970).

20. _____, V. Krejef, I. Grobec, and V. Perina. "Measurements on Random Ionization Waves (Irregular Striations) Using Space-Time Oscillograms." Czechoslovakian Journal of Physics, 16:65 (1966).

21. Robertson, A. G. "Drift Velocity of Low Energy Electrons in Argon at 293 and 90 K." Australian Journal of Physics, 30:39-49 (February 1977).

22. Rohlena, K., T. Ruzicka, and L. Pekarek. "A Theory of Low Current Ionization Waves in Inert Gases." Czechoslovakian Journal of Physics, 22:920-937 (1972).

23. Sicha, M., and V. Rezocova. "Study of the Ionization Rote Variations in the Ionization Waves in Plasma I." Czechoslovakian Journal of Physics, 20:356-361 (1970).

24. _____. "Influence of Small Amplitude Ionization Waves on the Distribution Function of Electrons in a low Current Neon Glow Discharge." Czechoslovakian ournal of Physics, 22:1019 (1972).

25. Stirand, O., V. Krejci, and L. Lasko. "New Method of Displaying Disturbance and Wave Propagation." Review of Scientific Instruments, 37:1481-1484 (1966).

26. Venzke, D. Beitrage Plamaphys, 10, 141 (1971).

27. Woolsey, G. S., K. G. Emeleus, J. M. Brown, J. J. G. McCloskey, and J. R. M. Coulter. "Moving Striations in Iodine Vapor." Discharge in Electronegative Gases. London: Taylor and Francis, Ltd. (1970).

Appendix A

Simple Stability Analysis

Many theoretical models now exist for glow discharges which are in close agreement with experimental results. D. H. Douglas-Hamilton and Silva A. Mani developed a model to explain instabilities caused by electron attachment in plasmas. In particular, the paper in which the model was explained dealt with instabilities associated with dissociative attachment that increased sharply with the electric field. They tested their model using an electron beam sustained discharge and found good agreement with their theory.

In this model, it is assumed that the current is predominantly carried by the electrons, so $j = en_e\mu_e E$, where μ_e is the electron mobility. Diffusion is considered negligible compared to attachment and recombination. The electron continuity equation is then

$$\frac{dn_e}{dt} = S - \beta n_e - \alpha n_e n_+ \qquad \text{(A-1)}$$

where S is the ionization source term, β is the attachment rate, and α is the recombination rate. β is assumed to be dependent upon the electric field while α and S are constant. The authors obtained the equation below as their final result.

$$S_{critical} = \frac{1}{\alpha}\left[E\,\frac{d\beta}{dE} - \beta\right]^2 \qquad \text{(A-2)}$$

Equation A-2 gives the condition for instability. In particular, for discharges with dissociative attachment, there will be an attachment induced ionization instability if the ionization rate falls below $S_{critical}$.

From equation 6 in the analysis section, the electron continuity equation for the discharge in this thesis is

$$\frac{dn_e}{dt} = k_i n_e n_a - k_r^e n_e n_+ - k_a n_e n_s + k_d n_- n_c \qquad \text{(A-3)}$$

The steady state condition simply replaces the left-hand term with zero. Perturbations are now introduced into (A-3) as described earlier in the analysis section.

Retaining only first order perturbations and simplifying through the steady state condition, equation A-6 becomes

$$\begin{aligned} -i\omega n_e = {} & k_i \tilde{n}_e n_a + \tilde{k}_i n_e n_a - k_r^e \tilde{n}_e n_+ - k_r^e n_e \tilde{n}_+ \\ & - \tilde{k}_r^e n_e n_+ - k_a \tilde{n}_c n_s - \tilde{k}_a n_e n_c \\ & + k_d \tilde{n}_- n_c + \tilde{k}_d n_- n_c \end{aligned} \qquad \text{(A-4)}$$

Perturbations in the various rate terms are taken with respect to E:

$$\tilde{k}_x = E' \frac{dk_x}{dE} + k_x \qquad \text{(A-5)}$$

Taking the limiting case of $n_e \tilde{\sim} n_+$ ($k_a \tilde{\sim} 0$), the steady state form of equation A-3 becomes

$$0 = k_i n_a n_e - k_r^e n_+^2 \qquad \text{(A-6)}$$

Solving for n_+ yields

$$n_+ = \left[\frac{k_i n_a n_e}{k_r^e}\right]^{\frac{1}{2}} \qquad \text{(A-7)}$$

Equation A-4 is now rewritten as

$$\begin{aligned} -i\omega n_e = {} & \tilde{k}_i n_e n_a - \tilde{k}_r^e n_e n_+ \; k_r^e n_e \tilde{n}_+ - \tilde{k}_a n_e n_s \\ & + \tilde{k}_d n_- n_c + (k_i \tilde{n}_e n_a - k_r^e \tilde{n}_e n_+ \\ & + k_d \tilde{n}_- n_c - k_a \tilde{n}_e n_s) \end{aligned} \qquad \text{(A-8)}$$

The terms within the parentheses can be dropped under steady state conditions. Substituting in equation A-7, and simplifying, equation A-8 becomes

$$\begin{aligned} \omega = i \Bigg[& -k_i^{\frac{1}{2}} \frac{n_a n_e}{k_r^e}^{\frac{1}{2}} \frac{\tilde{k}_r^e n_e}{\tilde{n}_e} + \frac{\tilde{k}_i n_e n_a}{\tilde{n}_e} \\ & - \frac{\tilde{k}_a n_e n_s}{\tilde{n}_e} + \frac{k_d n_- n_c}{\tilde{n}_e} \Bigg] \end{aligned} \qquad \text{(A-9)}$$

In the above equation, second order terms have again been ignored. If the terms in the bracket are negative in overall value, then the discharge will be stable. This can be written as

$$k_i^{\frac{1}{2}}\left(\frac{n_a n_e}{k_r^e}\right)^{\frac{1}{2}}\tilde{k}_r n_e > \tilde{k}_a n_e n_s - \tilde{k}_i n_e n_e - \tilde{k}_d n_- n_c \qquad \text{(A-10)}$$

or $$k_i > \frac{k_r^e}{n_a n_e^3 \tilde{k}_r^{e2}}\left[\tilde{k}_a n_e n_s - \tilde{k}_i n_e n_a - \tilde{k}_d n_- n_c\right]^2 \qquad \text{(A-11)}$$

Substituting equation A-5 into A-11 yields

$$k_i > \frac{k_r^e}{n_a n_e^3\left(E'\frac{dk_r^e}{dE} + k_r^e\right)^2}\left[n_e n_s\left(E'\frac{dk_a}{dE} + k_a\right)\right.$$

$$\left. - n_e n_a\left(E'\frac{dk_i}{dE} + k_i\right) - n_- n_c\left(E'\frac{dk_d}{dE} + k_d\right)\right]^2 \qquad \text{(A-12)}$$

Equation A-12 is similar to the results obtained by Mani and Hamilton. Differences arise from the added perturbations in all the rate terms as well as n_+. In addition, more rate processes were included in order to model the experimental discharge conditions.

Appendix B

Phase-Group Velocity Relation

Group velocity can be obtained from the disperson graphs developed from the current modulation data. The graphs showed a linear plot which can be described as

$$V_p = mf - V_{po} \tag{B-1}$$

where V_p is phase velocity, m is some constant denoting slope, f is frequency and V_{po} is the intercept on the vertical axis. V_{po} is given a negative sign since the intercept occurs at a negative value.

Phase velocity can be written as

$$V_p = w/k = \frac{2\pi f}{\frac{2\pi}{\lambda}} = f/(1/\lambda) \tag{B-2}$$

where λ is the wavelength. Group velocity, V_g, is given by:

$$V_g = \frac{dw}{dk} \tag{B-3}$$

Using the results of A-2, A-3 can be rewritten as:

$$V_g = \frac{df}{d(1/\lambda)} = \frac{df}{-\frac{d\lambda}{\lambda^2}} = \frac{-\lambda^2 df}{d\lambda} \tag{B-4}$$

An expression for the intercept, V_{po}, is now developed. Equation A-2 can be rewritten as:

$$\frac{V_p}{f} = \lambda \tag{B-5}$$

Equation A-5 is now differentiated.

$$d(V_{p/f}) = d\lambda \tag{B-6}$$

$$\rightarrow \frac{1}{f} dV_p - V_p \frac{df}{f^2} = d\lambda \tag{B-7}$$

Letting $V_p \rightarrow V_{po}$, then $dV_{po} = 0$ and equation A-7 becomes:

$$V_{po} = -f^2 \frac{d\lambda}{df} \tag{B-8}$$

Equation A-8 is now substituted into equation A-4 to obtain:

$$V_g = \frac{\lambda^2 f^2}{V_{po}} = \frac{V_p^2}{V_{po}} \tag{B-9}$$

At the intercept, $V_p = V_{po}$ and the final result becomes:

$$V_g = V_{po} \tag{B-10}$$

Hence, the group velocity is the intercept on the dispersion plot.

Vita

Darius S. Vunck was born on 24 January 1956 in Tokyo, Japan. After graduating from Piedmont Hills High School in San Jose, California, he entered the University of Santa Clara in 1974 majoring in physics. After joining the AFROTC in 1976, he transferred to San Jose State University where in 1978 he received his BS in physics and a commission in the USAF. His first duty assignment was to the Air Force Institute of Technology at Wright-Patterson AFB in June 1978.

Present Address: 3621 Vista del Valle
San Jose CA 95132

AD-A080 177 AIR FORCE INST OF TECH WRIGHT-PATTERSON AFB OH SCHOO--ETC F/G 7/4
EFFECTS OF SULFURHEXAFLUORIDE ON IONIZATION WAVES IN AN ARGON G--ETC(U)
DEC 79 D S VUNCK
UNCLASSIFIED AFIT/GEP/PH/79D-12 NL

2 OF 2
AD A080177

END
DATE FILMED
3-80
DDC

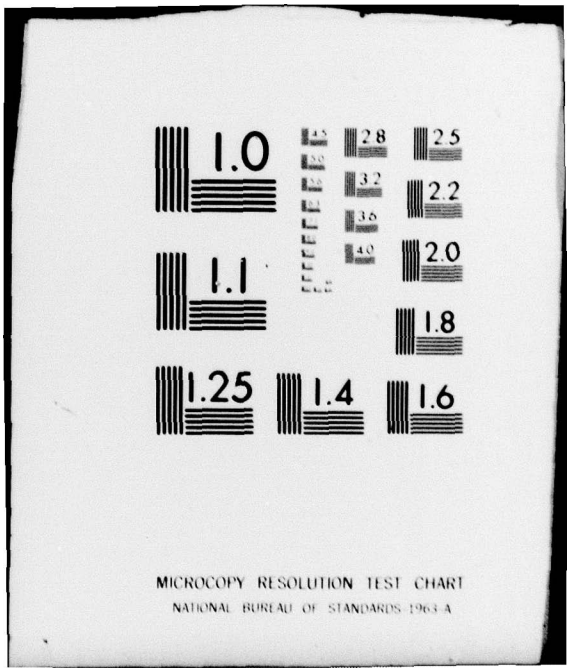
1.0
1.1
1.25
1.4
1.6
2.8
3.2
3.6
4.0
2.5
2.2
2.0
1.8
MICROCOPY RESOLUTION TEST CHART
NATIONAL BUREAU OF STANDARDS-1963-A

SECURITY CLASSIFICATION OF THIS PAGE (When Data Entered)

REPORT DOCUMENTATION PAGE	READ INSTRUCTIONS BEFORE COMPLETING FORM
1. REPORT NUMBER: AFIT/GEP/PH79D-12	2. GOVT ACCESSION NO. / 3. RECIPIENT'S CATALOG NUMBER
4. TITLE (and Subtitle): EFFECTS OF SULFURHEXAFLOURIDE ON IONIZATION WAVES IN AN ARGON GLOW DISCHARGE	5. TYPE OF REPORT & PERIOD COVERED: MS Thesis 6. PERFORMING ORG. REPORT NUMBER
7. AUTHOR(s): Darius S. Vunck, 2nd Lt, USAF	8. CONTRACT OR GRANT NUMBER(s)
9. PERFORMING ORGANIZATION NAME AND ADDRESS: Air Force Institute of Technology (AFIT-EN) Wright-Patterson AFB, Ohio 45433	10. PROGRAM ELEMENT, PROJECT, TASK AREA & WORK UNIT NUMBERS
11. CONTROLLING OFFICE NAME AND ADDRESS: Air Force Wright Aeronautical Laboratories (AFAPL/POE-3) Wright-Patterson AFB OH, 45433	12. REPORT DATE: December 1979 13. NUMBER OF PAGES: 96
14. MONITORING AGENCY NAME & ADDRESS(if different from Controlling Office)	15. SECURITY CLASS. (of this report): UNCLASSIFIED 15a. DECLASSIFICATION/DOWNGRADING SCHEDULE

16. DISTRIBUTION STATEMENT (of this Report)

Approved for public release; distribution unlimited

17. DISTRIBUTION STATEMENT (of the abstract entered in Block 20, if different from Report)

18. SUPPLEMENTARY NOTES

Approved for public release; IAW AFR 190-17

JOSEPH P. HIPPS, Major, USAF
Director of Public Affairs

19. KEY WORDS (Continue on reverse side if necessary and identify by block number)

Ionization Waves
Glow Discharge
Sulfurhexaflouride

20. ABSTRACT (Continue on reverse side if necessary and identify by block number)

Sulfurhexaflouride was added in trace amounts to a low pressure Argon glow discharge operated at 2.0 to 2.5 Torr and 1 to 30 mA. Using current modulation and voltage pulsing techniques, ionization waves were artifically driven and measured using a space-time correlation method developed by Stirand et al. It was found that the addition of SF_6 affected the dispersion properties of the ionization waves by directing the phase velocity so that the waves

DD FORM 1 JAN 73 1473 EDITION OF 1 NOV 65 IS OBSOLETE

UNCLASSIFIED

SECURITY CLASSIFICATION OF THIS PAGE (When Data Entered)

trended toward a forward wave type from the original backward waves found in pure Argon. In addition, the injection of CO as a detaching mechanism into the Argon/SF_6 discharge worked to reverse the effects of the SF_6.